JOURNAL OF GEOPHYSICAL RESEARCH, VOL. 117, A08111, doi:10.1029/2012JA017695, 2012

In situ detection of strong Langmuir turbulence processes in solar type III radio bursts

G. Thejappa,[1] R. J. MacDowall,[2] and M. Bergamo[1]

Received 7 March 2012; revised 29 May 2012; accepted 1 July 2012; published 29 August 2012.

[1] The high time resolution observations obtained by the WAVES experiment of the STEREO spacecraft in solar type III radio bursts show that Langmuir waves often occur as intense localized wave packets. These wave packets are characterized by short durations of only a few ms and peak intensities, which well exceed the supersonic modulational instability (MI) thresholds. These timescales and peak intensities satisfy the criterion of the solitons collapsed to spatial scales of a few hundred Debye lengths. The spectra of these wave packets consist of primary spectral peaks corresponding to beam-resonant Langmuir waves, two or more sidebands corresponding to down-shifted and up-shifted daughter Langmuir waves, and low frequency enhancements below a few hundred Hz corresponding to daughter ion sound waves. The frequencies and wave numbers of these spectral components satisfy the resonance conditions of the modulational instability (MI). Moreover, the tricoherences, computed using trispectral analysis techniques show that these spectral components are coupled to each other with a high degree of coherency as expected of the MI type of four wave interactions. The high intensities, short scale lengths, sideband spectral structures and low frequency spectral enhancements and, high levels of tricoherences amongst the spectral components of these wave packets provide unambiguous evidence for the supersonic MI and related strong turbulence processes in type III radio bursts. The implication of these observations include: (1) the MI and related strong turbulence processes often occur in type III source regions, (2) the strong turbulence processes probably play very important roles in beam stabilization as well as conversion of Langmuir waves into escaping radiation at the fundamental and second harmonic of the electron plasma frequency, f_{pe}, and (3) the Langmuir collapse probably follows the route of MI in type III radio bursts.

Citation: Thejappa, G., R. J. MacDowall, and M. Bergamo (2012), In situ detection of strong Langmuir turbulence processes in solar type III radio bursts, *J. Geophys. Res.*, *117*, A08111, doi:10.1029/2012JA017695.

1. Introduction

[2] This paper describes the strong Langmuir turbulence processes, namely, the supersonic modulational instability (MI) and collapsing Langmuir solitons observed in the source regions of solar type III radio bursts. These observations are from the WAVES experiment of the STEREO spacecraft [*Bougeret et al.*, 2008], which is designed to detect in situ waves as well as remote radio emissions over a wide frequency range. *Ginzburg and Zheleznyakov* [1958] were the first to suggest that (1) the electron beams accelerated during solar flares generate Langmuir waves at the local electron plasma frequency, $f_{pe}[Hz] = 9n_e^{1/2}$ by the bump-on-tail instability [*Bohm and Gross*, 1949] (n_e is the electron density in m^{-3}), and (2) these Langmuir waves are subsequently converted by some nonlinear processes into the observed type III radio emissions at the fundamental and second harmonic of the local electron plasma frequency, f_{pe}. Although this hypothesis has been confirmed by the in situ detection of type III burst associated electron beams [*Lin*, 1970; *Lin et al.*, 1973, 1981; *Ergun et al.*, 1998], and Langmuir waves [*Gurnett and Anderson*, 1976, 1977; *Lin et al.*, 1986; *Gurnett et al.*, 1993; *Thejappa et al.*, 1993a, 1993b, 1999; *Hospodarsky and Gurnett*, 1995; *Thejappa and MacDowall*, 1998; *Henri et al.*, 2009], several issues remain unresolved.

[3] *Sturrock* [1964] was the first to pose the following question: How does the electron beam preserve the bump-on-tail distribution over 1 AU and beyond against the "quasi-linear relaxation" or "plateauing", that is known to deplete all the streaming energy within 100 km or less? Here we should note that Sturrock considered a special case of an infinitely extended homogeneous plasma, and neglected the effects of re-acceleration of beam particles by Langmuir waves. Several authors [*Zaitsev et al.*, 1972, 1974; *Takakura*

[1]Department of Astronomy, University of Maryland, College Park, Maryland, USA.
[2]NASA Goddard Space Flight Center, Greenbelt, Maryland, USA.

Corresponding author: G. Thejappa, Department of Astronomy, University of Maryland, College Park, MD 20742, USA. (thejappa.golla@nasa.gov)

0148-0227/12/2012JA017695

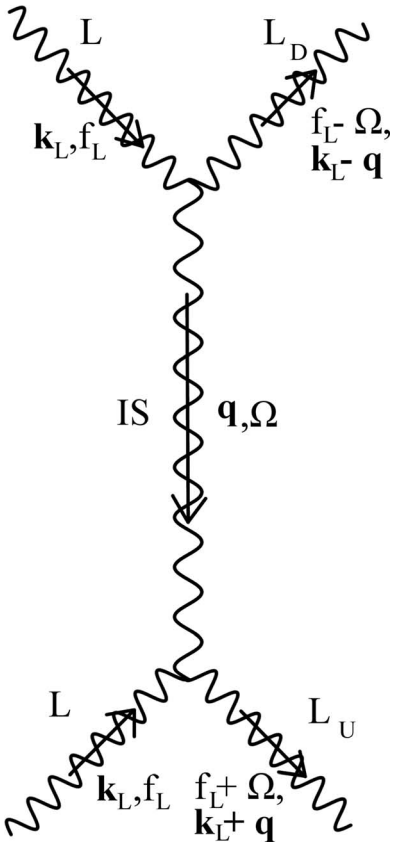

Figure 1. Schematic picture of the modulational instability (MI). Two beam excited Langmuir waves L are scattered into down-shifted (Stokes) L_D and up-shifted (anti-Stokes) L_U sidebands through the exchange of ion sound waves (IS). The frequencies and wave numbers of the beam excited Langmuir, and daughter ion sound, Stokes, and anti-Stokes modes are (f_L, k_L), (Ω, q), ($f_L - \Omega$, $k_L - q$), and ($f_L + \Omega$, $k_L + q$), respectively.

and Shibahashi, 1976; *Magelssen and Smith*, 1977; *Escande and de Genouillac*, 1978] have treated the wave particle interactions self-consistently all along the path of the inhomogeneous beam, and claimed that the continuous emission and reabsorption of waves enable the beam to survive over the distances of order of ∼1 AU and more. However, the Langmuir wave intensities predicted by the inhomogeneous quasi-linear theories are also subject to wave-wave interactions.

[4] In the context of homogeneous beam-plasma interaction, *Kaplan and Tsytovich* [1968] suggested that the induced scattering of Langmuir waves off ion clouds, which acts as the electrostatic decay of Langmuir waves into backscattered Langmuir waves and forward-going ion sound waves when $T_e > T_i$ (T_e and T_i are the electron and ion temperatures, respectively) can stabilize the beam; these authors considered only the mono energetic beam and isotropic distribution of waves. Although some signatures of the electrostatic decay are detected in type III source regions [*Lin et al.*, 1986; *Gurnett et al.*, 1993; *Thejappa et al.*, 1995, 2003; *Thejappa and MacDowall*, 1998; *Hospodarsky and Gurnett*, 1995; *Henri et al.*, 2009], if the assumption of mono energetic beam and isotropic distribution of waves is relaxed, the net scattering of waves out of resonance with the beam by the induced scattering becomes too slow to prevent quasi-linear relaxation [*Zheleznyakov and Zaitsev*, 1970; *Heyvaerts and de Genouillac*, 1974].

[5] The supersonic MI, which is popularly known as the oscillating two stream instability (OTSI) [*Papadopoulos et al.*, 1974; *Smith et al.*, 1979; *Goldstein et al.*, 1979] and, soliton formation and Langmuir collapse [*Zakharov*, 1972; *Nicholson et al.*, 1978; *Goldman*, 1983] are suggested as the most effective beam stabilization mechanisms. These strong Langmuir turbulence processes are the focus of several theoretical studies [*Zakharov*, 1972; *Goldman*, 1984; *Robinson*, 1997], computer simulations [*Bardwell and Goldman*, 1976; *Nicholson et al.*, 1978; *Degtyarev et al.*, 1980; *Doolen et al.*, 1985; *Russell et al.*, 1988] and experimental investigations [*Whelan and Stenzel*, 1981; *Michel et al.*, 1982; *Wong and Cheung*, 1984; *Cheung and Wong*, 1985a, 1985b; *McFarland and Wong*, 1997, 2001; *Vyacheslavov et al.*, 2002] because of the fundamental nature of the problem [*Zakharov*, 1972; *Krasnoselskikh and Sotnikov*, 1977], and practical importance in fields, such as the laser heating of pellets [*Montgomery et al.*, 1999], ionospheric modification experiments [*DuBois et al.*, 1993], and several astrophysical applications [*Galeev and Krasnoselskikh*, 1976, 1978; *Gurnett et al.*, 1981; *Pelletier et al.*, 1988; *Balikhin et al.*, 1989; *Kellogg et al.*, 1999].

[6] As shown in Figure 1, MI excites a low frequency ion density perturbation of frequency and wave number (Ω, q), which can be either a quasi-mode or a freely propagating ion sound wave. This ion sound wave can beat with two of the beam-resonant Langmuir waves with frequencies and wave numbers (f_L, k_L) and produce high frequency sidebands in the non resonant region with frequencies and wave numbers ($f_L - \Omega$, $\vec{k_L} - \vec{q}$) (Stokes mode) and ($f_L + \Omega$, $\vec{k_L} + \vec{q}$) (anti-Stokes mode). The nonlinear effect responsible for MI is the density cavity dug by the action of the ponder motive force of the Langmuir wave electric field, which in turn traps the waves thus deepening it still further. Usually, the Langmuir wave bunch localized in the corresponding density cavity is referred to as the Langmuir soliton. The spatial collapse, on the other hand, occurs due to intensification of the Langmuir wave packet in the self generated density cavity [*Zakharov*, 1972].

[7] *Gurnett et al.* [1981] were the first to report the Voyager observations of the possible evidence for MI and spatial collapse of Langmuir waves in the Jovian foreshock region. However, in this case, the daughter ion sound waves were not detected, and the intensities of Langmuir waves were well below the strong turbulence thresholds. The Ulysses observations of Langmuir waves in the form of intense millisecond spikes were interpreted in terms of Langmuir collapse [*Kellogg et al.*, 1992; *Thejappa et al.*, 1993b]. However, in this case, there were some instrumental uncertainties regarding millisecond spikes. We have reported the observations of the coexistence of strong and weak Langmuir turbulence processes [*Thejappa and MacDowall*, 1998], envelope solitons formed as a result of subsonic MI [*Thejappa et al.*, 1999] and ion-sound waves radiated by the burnt-out cavitons left behind by the collapse events

[*Thejappa and MacDowall*, 2004] in type III sources. However, the envelope soliton does not correspond to the concept of physical collapse of Langmuir waves because of its relatively large spatial scale $S \gg \lambda$ and low intensity (λ is the wavelength of the Langmuir wave). Of much greater interest from the point of collapse is the large-amplitude Langmuir soliton formed in the regime $\frac{W_L}{n_e T_e} > (k_L \lambda_{De})^2$ and $\frac{W_L}{n_e T_e} > \frac{m_e}{m_i}$, with $S < \lambda = \frac{2\pi}{k_L}$, which corresponds to the supersonic MI [*Zakharov et al.*, 1985]. Here $\frac{W_L}{n_e T_e}$ is the normalized energy density of Langmuir waves, m_e and m_i are the electron and ion masses, λ_{De} is the electron Debye length and k_L is the wave number of the Langmuir waves. Even after years of comprehensive in situ high time resolution measurements of the wave and beam parameters [*Lin et al.*, 1986; *Kellogg et al.*, 1992; *Gurnett et al.*, 1993; *Thejappa et al.*, 1993a, 1993b, 1996, 1999, 2003; *Hospodarsky and Gurnett*, 1995; *Thejappa and MacDowall*, 1998, 2004; *Ergun et al.*, 2008; *Henri et al.*, 2009], the evidence for the Langmuir collapse has proved to be extremely elusive.

[8] Recently, *Thejappa et al.* [2012a] reported the high time resolution observations of a very intense localized Langmuir wave packet in the source region of a type III radio burst from the improved Time Domain Sampler (TDS) of the STEREO/WAVES experiment (improved over that of all similar high time resolution receivers flown in earlier spacecraft in precision, linearity, sample length and rate [*Kellogg et al.*, 2009]). The characteristics of this wave packet include: (1) the normalized peak energy density $\frac{W_L}{n_e T_e}$ which is well above the threshold for the supersonic MI, (2) timescale of only $\sim$3 ms, and (3) spectrum containing the resonant peak at the local electron plasma frequency, f_{pe}, sidebands at frequencies slightly lower than f_{pe} (Stokes mode) as well as slightly higher than f_{pe} (anti-Stokes mode), and low frequency enhancement below a few hundred Hz, which satisfy the frequency and wave number matching rules of MI. The spatial scale determined using the observed timescale of the wave packet is less than the spatial scale derived using the normalized peak intensity, which indicates that the wave packet is probably the Langmuir soliton collapsed to a few hundred Debye lengths. These observations were interpreted in terms of the oscillating two stream instability (OTSI), which is nothing but the supersonic MI and collapsing Langmuir soliton. In a separate study, *Thejappa et al.* [2012b] applied the trispectral analysis technique and showed that the spectral components of this wave packet are coupled to each other with a high degree of phase coherency (high tricoherence).

[9] In this study, we present a detailed analysis of high time resolution observations of Langmuir wave packets associated with four other type III events. These TDS events represent some of the most intense localized Langmuir wave packets ever detected in type III bursts. The characteristics of these wave packets indicate that MI and associated strong turbulence processes occur in type III radio bursts. The implications of this study include (1) the strong turbulence processes probably play important roles in beam stabilization as well as conversion of Langmuir waves into escaping fundamental and harmonic radio emissions, and (2) the Langmuir collapse in type III sources probably occurs via MI as suggested by *Zakharov* [1972]. In section 2, we present the observations, in section 3, we present the discussion, and in section 4, we present the conclusions.

2. Observations

[10] The STEREO/WAVES experiment [*Bougeret et al.*, 2008] is uniquely suited to study the nonlinear processes associated with solar type III radio bursts. It can detect a variety of in situ waves as well as remote radio emissions over a wide frequency range. Data from three of the SWAVES instruments are pertinent to this study: the high frequency receiver (HFR), low frequency receiver (LFR) and time domain sampler (TDS).

[11] 1. *High frequency receiver (HFR)*- The HFR measures the remote electric field signals over the frequency range 125 kHz - 16.025 MHz with 50 kHz increments. The total dynamic range of the HFR is 80 dB and its sensitivity at the preamplifier input is 6 $\text{nVHz}^{-1/2}$.

[12] 2. *Low frequency receiver (LFR)*- The LFR is a direct conversion receiver for spectral processing from 2.5 kHz up to 160 kHz. The frequency range is divided into three 2-octave bands A (2.5–10) kHz, B (10–40) kHz and C (40–160) kHz. The LFR covers a broad dynamic range with a constant amplitude resolution over the whole range, i.e., it adjusts its gain according to the input level. Automatic Gain Control (AGC) determines the receiver gain on a logarithmic scale as a function of the input level. The LFR analog front end normalizes the signal amplitude with an allowable gain variation of 80 dB. Combined with 12-bit analog to digital converters, the LFR provides a total dynamic range of 120 dB. The LFR sensitivity is 6 $\text{nVHz}^{-1/2}$ at the preamplifier input.

[13] 3. *Time domain sampler (TDS)*- The TDS is intended primarily for the study of Langmuir waves at the local electron plasma frequency, f_{pe}. It gathers events on three channels simultaneously connected to three orthogonal antennas and to a fourth pseudo-dipole channel obtained by taking the difference of any two monopoles. The TDS has programmable sampling rates with events of maximum length of 16 kilo samples, with possible rates of 250,000, 125,000, 31,250 and 7,812.5 samples per second. The maximum event duration can be as long as 2 s. The use of a 16 bit linear A/D converter provides sufficient dynamic range with better fidelity. The long durations of the TDS events enable us to determine the frequency components of the wave packets accurately. The gain is linear in the frequency range of interest, from typical electron cyclotron frequency, $f_{ce} \sim 100$ Hz to typical electron plasma frequency $f_{pe} \sim 30$ kHz.

[14] In the data, we have identified four type III events, for which the radio emissions drift from high frequencies to f_{pe} or $2f_{pe}$, where f_{pe} is the local electron plasma frequency. The Langmuir wave packets captured by the TDS during these events form the observational basis for the current study. These type III events occurred on 2011 December 19 (event I), 2012 February 12 (event II), 2009 July 18 (event III) and 2006 December 5 (event IV). We assign a typical value of $\sim 10^5$ K for the electron temperature T_e for all four events. Here we note that owing to an unfortunate malfunction of the electron experiment, STEREO does not measure the electron temperature, T_e. For the solar wind speed (v_{sw}), we use the

values of 450 km s^{-1}, 500 km s^{-1} and 500 km s^{-1} for events I, II and III, respectively. These values are from the STEREO/PLASTIC experiment [*Galvin et al.*, 2008]. Since the data of solar wind are not available from the STEREO spacecraft for 2006 December 5 event (event IV), we use a value v_{sw} = 315 km s^{-1} obtained by the WIND/SWE experiment [*Ogilvie et al.*, 1995]; the STEREO A, B and WIND were very close to each other during this event. We have deduced the electron densities, n_e of the solar wind as $\sim 4.5 \times 10^6$ m^{-3}, $\sim 2.4 \times 10^6$ m^{-3}, $\sim 5 \times 10^6$ m^{-3} and $\sim 1.2 \times 10^7$ m^{-3} from the frequencies of the dominant spectral peaks of the waveforms of ~19.12 kHz, ~14 kHz, ~20.1 kHz and ~31.6 kHz (see, Figures 5, 9, 13, and 17); these frequencies are assumed to correspond to local electron plasma frequencies, $f_{pe}[Hz] = 9n_e^{1/2}$, (n_e is in m^{-3}) during events I to IV, respectively.

[15] The solarsoft solar activity reports indicate that events I to IV are likely associated with active regions of N18W28, N29E85, N22W81 and S06E71, respectively. For the electron density n_e (m^{-3}), we assume the Radio Astronomy Explorer (RAE) density model [*Fainberg and Stone*, 1971]:

$$n_e = n_0 r^{-a}, \tag{1}$$

where $n_0 = 5.52 \times 10^{13}$, $a = 2.63$ and r is the solar altitude (in units of $R_\odot$). If one assumes that the type III bursts are excited at $2f_{pe}$ by the electron beams traveling along the spiral magnetic field lines with velocities β (units of velocity of light c), the frequency drifts can be expressed as [*Papagiannis*, 1971]

$$\frac{df}{dt} = -\frac{a\beta c}{2(1-\beta\cos\phi)R_\odot\left(81\times10^{-6}\right)^{1/a}} f^{(a+2)/a}, \tag{2}$$

where c is the velocity of light, ϕ is the angle of exciter direction to Sun-Spacecraft line, and f is the midpoint of frequency interval *df*. This expression is derived assuming that the type III electrons propagate along the Parker's spiral field lines. By fitting the frequency drift curves to the dynamic spectra, we can estimate the beam speeds v_b as ~0.3*c*, ~0.28*c*, ~0.37*c*, and ~0.35*c* for events I to IV, respectively. Since, the pitch angle scattering increases the path length traveled by electrons by a factor of α = 1.3 to 1.7 [*Alvarez et al.*, 1975; *Lin et al.*, 1973; *Fokker*, 1984], the actual beam speeds are probably much greater than these estimated speeds.

[16] Using these values, we estimate: (1) the Debye lengths $\lambda_{De} = 69T_e^{1/2}n_e^{-1/2}$ as ~10.3 m, ~14 m, ~9.8 m and ~6.2 m, (2) wave numbers of beam-excited Langmuir waves $k_L = \frac{\omega_{pe}}{v_b}$ as $\sim 1.3 \times 10^{-3}$ m^{-1}, $\sim 1 \times 10^{-3}$ m^{-1}, $\sim 1.1 \times 10^{-3}$ m^{-1} and $\sim 1.9 \times 10^{-3}$ m^{-1}, and (3) $k_L\lambda_{De}$ as $\sim 1.4 \times 10^{-2}$, $\sim 1.5 \times 10^{-2}$, $\sim 1.1 \times 10^{-2}$, and $\sim 1.2 \times 10^{-2}$, for events I to IV, respectively.

2.1. December 19, 2011 (Event I)

[17] In Figure 2, we present the frequency-time spectrogram illustrating the type III radio burst. The data used in the spectrogram are from the HFR as well as LFR of the WAVES experiment of the STEREO A spacecraft. The intense emission drifting from ~5 MHz to ~28 kHz is the type III burst. This is identified as the local event because of its drift from very high frequencies all the way to twice the local electron plasma frequency f_{pe}. Since type III emission frequencies depend on the radially decreasing electron density n_e, these bursts occur at lower frequencies at later times. The in situ wave data acquired during local type III events are extensively used to study the non-linear plasma processes [*Lin et al.*, 1986; *Kellogg et al.*, 1992; *Gurnett et al.*, 1993; *Thejappa et al.*, 1993a, 1999, 2003; *Hospodarsky and Gurnett*, 1995; *Henri et al.*, 2009].

[18] In association with the type III radio burst, the LFR has detected Langmuir waves (non-drifting emissions in the 19–25 kHz frequency range) generated probably by the solar flare electron beam. In Figure 3, we present the frequency-time spectrogram of Langmuir waves. As seen from this spectrogram, the frequencies of these emissions fall suddenly from ~28 kHz to ~19 kHz at ~13:45 UT, and remain at that frequency for almost 35 min, and, then jump suddenly to ~25 kHz at ~14:20 UT. These abrupt changes in the frequencies of Langmuir waves are probably due to some density structure in the solar wind. As seen from this spectrogram, at any given instant, the Langmuir waves show substantial frequency spreading of ~8 kHz, which is indicative of nonlinear frequency broadening. The Langmuir wave burst corresponding to the TDS event of the present study is shown by an arrow in this figure.

[19] Time Domain Sampler (TDS) has resolved these Langmuir waves as highly localized wave packets. Each of these wave packets contains 16384 samples with an acquisition rate of 250,000 samples per second (a time step of 4 μs for a total duration of 65 ms). In Figure 4, we present one of the most intense wave packets detected during this type III event. This event is selected because of its sideband spectral structure, even though it is slightly weaker than the TDS events, which occur later at ~13:20 UT. The peak electric field strength E_L of this event is 34.6 mVm^{-1} and its $\frac{1}{e}$-power duration τ is ~5.7 ms. These values yield (1) the normalized peak energy density $\frac{W_L}{n_eT_e} = \frac{\epsilon_0 E_L^2}{2n_eT_e} \simeq 8.5 \times 10^{-4}$ for E_L = 34.6 mVm^{-1}, $n_e = 4.5 \times 10^6$ m^{-3} and $T_e = 10^5$ K, and (2) the spatial scale of the field structure $S \sim 250\lambda_{De}$ (using the relation $S \sim \tau v_{sw}$) for τ = 5.7 ms, v_{sw} = 450 km s^{-1} and $\lambda_{De} \sim$ 10.3 m. Since the E_x, E_y and E_{x-y} signals are weaker and show the same general features as the E_z signal, we analyze only the E_z signal. We justify one-dimensional treatment by assuming that these Langmuir wavefields are probably aligned along the ambient magnetic field.

[20] In Figure 5, we show the spectral characteristics of this wave packet. Figure 5a shows the total spectrum of the waveform from 0 to 65 kHz. The primary spectral peak at ~19.12 kHz probably corresponds to Langmuir waves excited by the beam at the local electron plasma frequency, f_{pe}. Figure 5b shows the narrow logarithmic spectrum around this primary spectral peak. This spectrum contains an intense peak (L) at $f_{pe} \sim$ 19.12 kHz, corresponding to the beam excited Langmuir wave, a down-shifted sideband (D) at ~19 kHz which is slightly less than f_{pe} and an up-shifted sideband (U) at ~19.3 kHz, which is slightly higher than f_{pe}. Figure 5c shows linear spectrum below 1.5 kHz. A clear enhancement below 200 Hz seen in this low frequency spectrum probably corresponds to ion-sound waves.

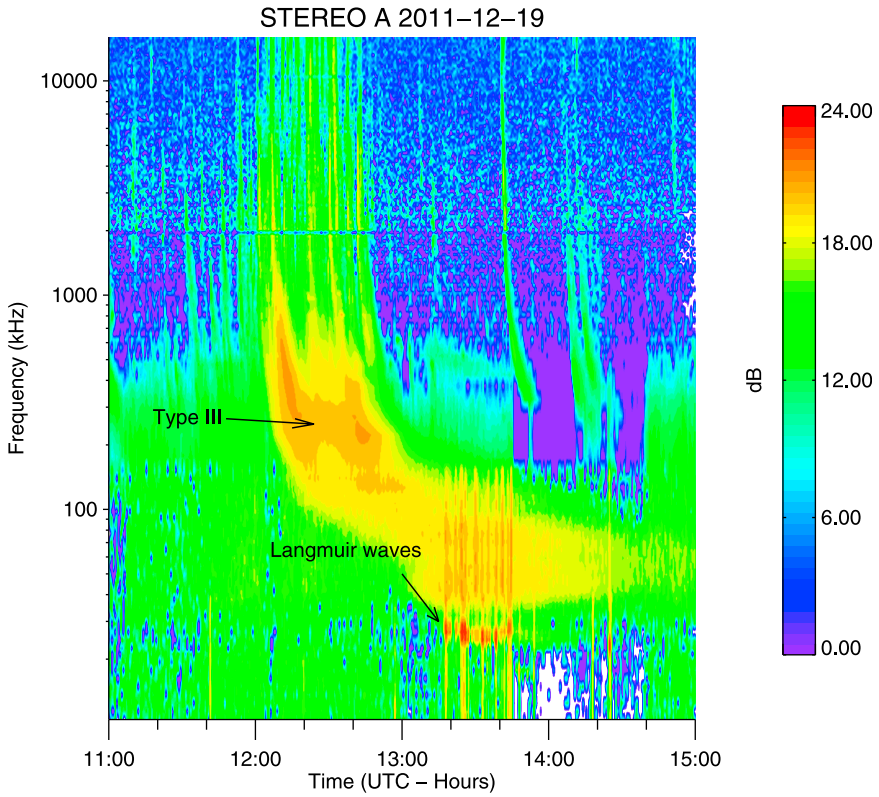

Figure 2. Dynamic spectrum of the wave activity observed by the WAVES experiment of STEREO A spacecraft from 11:00 to 15:00 UT on 2011 December 19. The fast drifting emission from ~5 MHz down to ~28 kHz is identified as the local type III radio burst, and the non-drifting emissions in the 19–25 kHz frequency band are identified as the Langmuir waves.

2.2. February 11, 2012 (Event II)

[21] In Figure 6, we present the dynamic spectrum of the second type III event and associated Langmuir waves, observed on February 11, 2012 by the STEREO B spacecraft. The fast drifting type III burst and the non-drifting Langmuir wave emissions are clearly seen in this dynamic spectrum. In Figure 7, we present the frequency-time spectrogram in a narrow frequency range, which shows the clumpy Langmuir waves with substantial frequency spreading. In this figure, the Langmuir wave burst corresponding to the TDS event of the present study is shown by an arrow. In Figure 8, we present one of the most intense wave packets detected by the TDS during this type III event. This TDS event is characterized by the peak electric field strength E_L of 44.73 mVm^{-1} and $\frac{1}{e}$-power duration τ of ~7.9 ms. These values yield: (1) $\frac{W_L}{n_e T_e} \simeq 2.6 \times 10^{-3}$ for $E_L = 44.7$ mVm^{-1}, $n_e = 2.4 \times 10^6$ m^{-3} and $T_e = 10^5$ K, and (2) $S \sim 282\lambda_{De}$ for the measured values of τ = 7.9 ms and v_{sw} = 500 km s^{-1}. In Figure 9, we show the spectral characteristics of this wave packet. The total spectrum of the waveform from 0 to 65 kHz is shown in Figure 9a, where the primary spectral peak at ~14 kHz corresponds probably to beam excited Langmuir wave at f_{pe}. The narrow logarithmic spectrum around this primary peak (L) in Figure 9b shows two sidebands, Stokes peak (D) at ~13.78 kHz (which is slightly less than f_{pe}), and an anti-Stokes peak (U) at ~14.25 kHz (which is slightly higher than f_{pe}). In Figure 9c, we present the low frequency spectrum, which shows a clear enhancement ≤250 Hz corresponding to ion-sound waves.

2.3. July 18, 2009 (Event III)

[22] In Figure 10, we present the dynamic spectrum of the third local type III event and associated Langmuir waves. This event was observed by the STEREO A spacecraft on July 18, 2009. In Figure 11, we present the frequency-time spectrogram of the Langmuir waves, where the arrow shows the location of the TDS event of the present study. Here we note that even though this TDS event (Figure 12) is slightly weaker than some of the later events, it is included in the present analysis because of its sideband spectral structure. This TDS event is characterized by the peak electric field E_L of 70.9 mVm^{-1} and $\frac{1}{e}$-power duration τ of ~10 ms. These values yield: (1) $\frac{W_L}{n_e T_e} \simeq 3.2 \times 10^{-3}$ for E_L = 70.9 mVm^{-1}, $n_e = 5 \times 10^6$ m^{-3} and $T_e = 10^5$ K, and (2) $S \sim 512\lambda_{De}$ for the measured values of τ = 10 ms and v_{sw} = 500 km s^{-1}. Figure 13 presents the spectral characteristics of this wave packet. Figure 13a shows the total spectrum of the waveform from 0 to 65 kHz, where the dominant spectral peak at ~20.1 kHz corresponds to Langmuir waves excited by the electron beam at f_{pe}. Figure 13b shows the narrow logarithmic spectrum around this intense peak (L), which contains two sidebands: a Stokes peak (D) at ~19.85 kHz (which is slightly less than f_{pe}), and an anti-Stokes peak (U) at ~20.32 kHz (which is slightly higher than f_{pe}). In Figure 13c,we present the low frequency spectrum of this

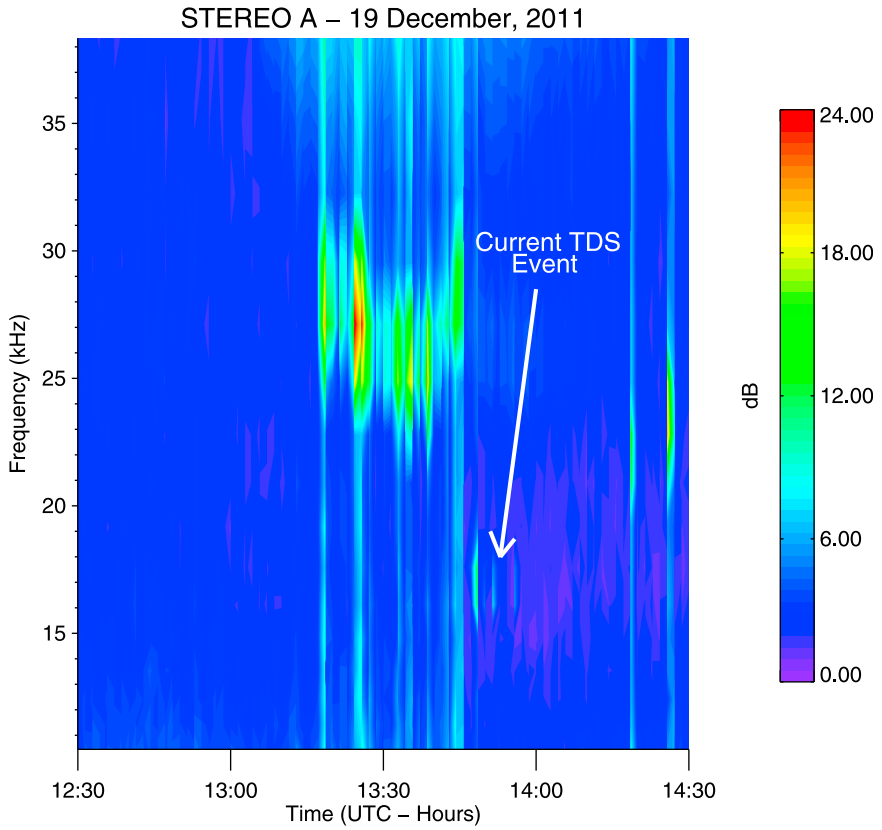

Figure 3. Frequency-time spectrogram of the Langmuir wave activity associated with the type III burst of December 19, 2011. These waves are very bursty and show substantial frequency broadening. As seen from this spectrogram, the frequencies of these emissions fall suddenly from ~28 kHz to ~19 kHz at ~13:45 UT, and remain at that frequency for almost 35 min, and, then jump suddenly to ~25 kHz at ~14:20 UT. These abrupt changes in the frequencies are probably due to some unknown density structure in the solar wind. The location of the current TDS event is shown by the arrow.

wave packet, which shows a clear enhancement ≤250 Hz corresponding to ion-sound waves.

2.4. December 5, 2006 (Event IV)

[23] In Figure 14, we present the dynamic spectrum of the fourth local type III event and associated Langmuir waves, observed by the STEREO B spacecraft. Here the fast drifting emission from ~10:00 to ~12:30 UT is the type III burst, and the non-drifting emissions in the 28–32 kHz frequency range are the Langmuir waves. In Figure 15, we present the frequency-time spectrogram in a narrow frequency band, which clearly shows that the Langmuir waves are very bursty and show substantial frequency spreading ~10 kHz. The arrow shows the Langmuir wave burst corresponding to the TDS event of the present study.

[24] In Figure 16, we present one of the most intense waveforms detected during this type III event, which contains several modulated structures. The most intense structure is characterized by E_L = 69.7 mVm^{-1} and $\tau \sim 7$ ms. These measured parameters yield: (1) $\frac{W_L}{n_e T_e} \simeq 1.3 \times 10^{-3}$ for E_L = 69.7 mVm^{-1}, $n_e = 1.23 \times 10^7$ m^{-3} and $T_e = 10^5$ K, and (2) $S \sim 355\lambda_{De}$ for the measured values of τ = 7 ms and v_{sw} = 315 km s^{-1}. In Figure 17, we show the spectral characteristics of this wave packet, where Figure 17a shows the total spectrum from 0 to 65 kHz. The dominant spectral peak at ~31.6 kHz in Figure 17a corresponds to Langmuir waves excited by the electron beam at the local electron plasma frequency, f_{pe}, which corresponds to n_e of 1.23×10^7 m^{-3}. The narrow logarithmic spectrum around this dominant spectral peak (L) as shown in Figure 17b contains several secondary peaks. The peaks at frequencies slightly less than f_{pe} (Stokes modes) are denoted as D_1 and D_2, and peaks at frequencies slightly higher than f_{pe} (anti-Stokes modes) are denoted as U_1, U_2 and U_3. The low frequency spectrum as seen in Figure 17c clearly shows the ion acoustic wave associated enhancement ≤200 Hz.

3. Discussion

[25] In Table 1, we present the summary of observations. The normalized peak energy density $\frac{W_L}{n_e T_e} = \frac{\epsilon_0 E_L^2}{2 n_e T_e}$ controls the non-linear beam-plasma interactions. If

$$\frac{W_L}{n_e T_e} \geq (k_L \lambda_{De})^2, \tag{3}$$

then the dominant nonlinear beam-plasma interactions are the modulational instability [*Papadopoulos et al.*, 1974] and the fully developed soliton formation and collapse

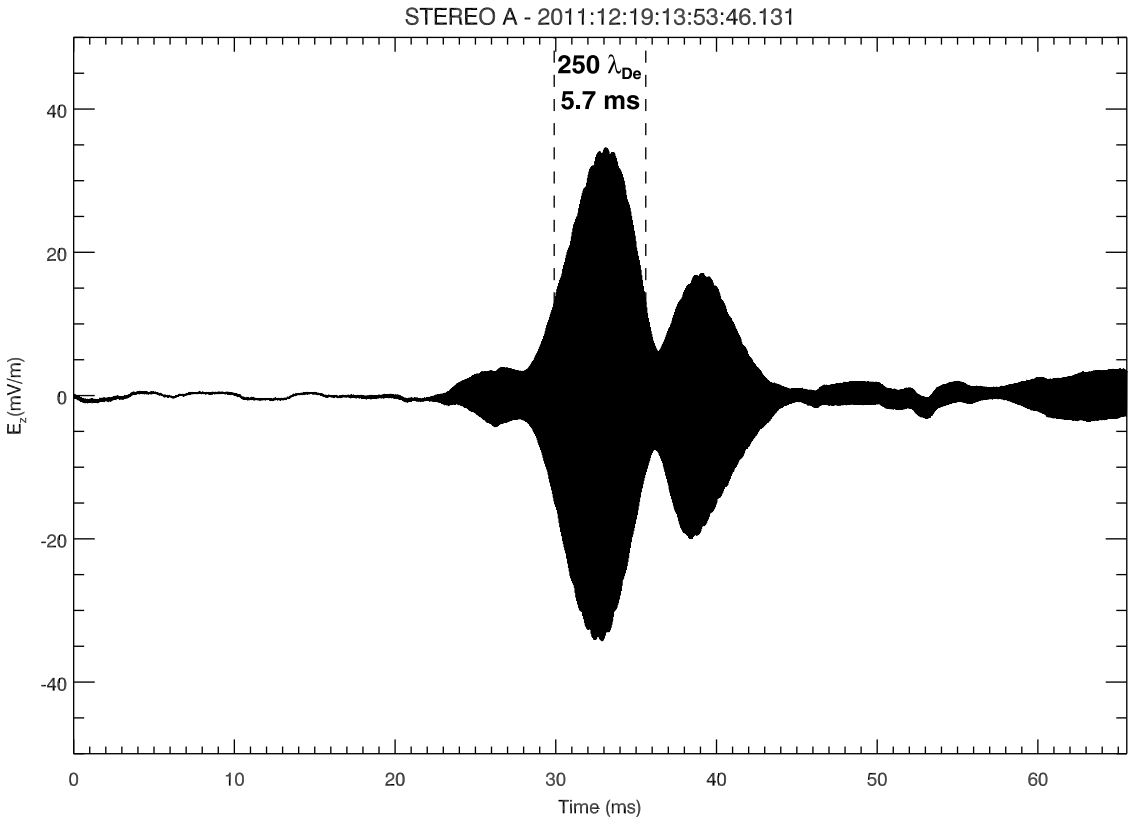

Figure 4. One of the most intense Langmuir wave packets captured by the Time Domain Sampler (TDS) during type III event of Figure 2. The $\frac{1}{e}$ power duration of 5.7 ms is equivalent to the spatial scale of ~250 Debye lengths (λ_{De}). The peak intensity E_L of this wave packet is ~34.6 mVm^{-1}.

[*Nicholson et al.*, 1978]. In the present case, this condition is easily satisfied, since the observed $\frac{W_L}{n_e T_e}$ of 8.5×10^{-4}, 2.6×10^{-3}, 3.2×10^{-3} and 1.3×10^{-3} are well above the estimated $(k_L \lambda_{De})^2$ values of 1.9×10^{-4}, 2.2×10^{-4}, 1.2×10^{-4} and 1.4×10^{-4}, for the events I to IV, respectively. This suggests that the strong turbulence processes can occur, and, therefore, in the context of present observations, we examine MI [*Zakharov*, 1972; *Papadopoulos et al.*, 1974; *Smith et al.*, 1979; *Goldstein et al.*, 1979], and related soliton formation and Langmuir collapse [*Zakharov*, 1972; *Nicholson et al.*, 1978; *Goldman*, 1984].

[26] For the events of the present study, the inequality

$$k_L \leq \left(\frac{m_e}{m_i}\right)^{1/2} k_D \tag{4}$$

is easily satisfied, since $\left(\frac{m_e}{m_i}\right)^{1/2} k_D$ are of 2.3×10^{-3} m^{-1}, 1.7×10^{-3} m^{-1}, 2.4×10^{-3} m^{-1} and 3.8×10^{-3} m^{-1}, whereas, the wave numbers of the beam excited Langmuir waves, k_L are $\sim 1.3 \times 10^{-3}$ m^{-1}, $\sim 1 \times 10^{-3}$ m^{-1}, $\sim 1.1 \times 10^{-3}$ m^{-1} and $\sim 1.9 \times 10^{-3}$ m^{-1} for the events I to IV, respectively ($m_{e,i}$ are the electron and ion masses, respectively, and $k_D = \frac{1}{\lambda_{De}}$). We have estimated the beam speeds for a smooth spiral. The pitch angle scattering is known to increase the path length of electrons by a factor of $\alpha = 1.3$ to 1.7 [*Alvarez et al.*, 1975; *Lin et al.*, 1973]. This implies that the beam speeds, corrected for the pitch angle scattering will be much more favorable for MI and spatial collapse.

[27] As far as the inequality $\frac{W_L}{n_e T_e} > \frac{m_e}{m_i}$ is concerned, it is also easily satisfied for all four events, since the observed $\frac{W_L}{n_e T_e}$ are 8.5×10^{-4}, 2.7×10^{-3}, 3.2×10^{-3} and 1.3×10^{-3}, whereas, $\frac{m_e}{m_i}$ is $\sim 5.5 \times 10^{-4}$. This indicates that the observed wave packets are in the regime of supersonic modulational instability (MI) as shown schematically in Figure 18. The different regimes of Langmuir wave saturation mechanisms are discussed by *Zakharov et al.* [1985].

[28] The growth rate of supersonic MI

$$\frac{\Gamma}{\omega_{pe}} = \left(\frac{m_e}{3m_i} \frac{W_L}{n_e T_e}\right)^{1/2} \tag{5}$$

can be estimated as $\sim 4 \times 10^{-4}$, $\sim 7 \times 10^{-4}$, $\sim 7.7 \times 10^{-4}$ and $\sim 4.8 \times 10^{-4}$ for the observed $\frac{W_L}{n_e T_e}$ of 8.5×10^{-4}, 2.7×10^{-3}, 3.2×10^{-3} and 1.3×10^{-3} corresponding to the events of Figures 4, 8, 12, and 16, respectively. On the other hand, the bandwidth of the beam-excited Langmuir waves

$$\frac{\Delta\omega}{\omega_{pe}} = 3(k_L \lambda_{De})^2 \frac{\Delta k_L}{k_L} \tag{6}$$

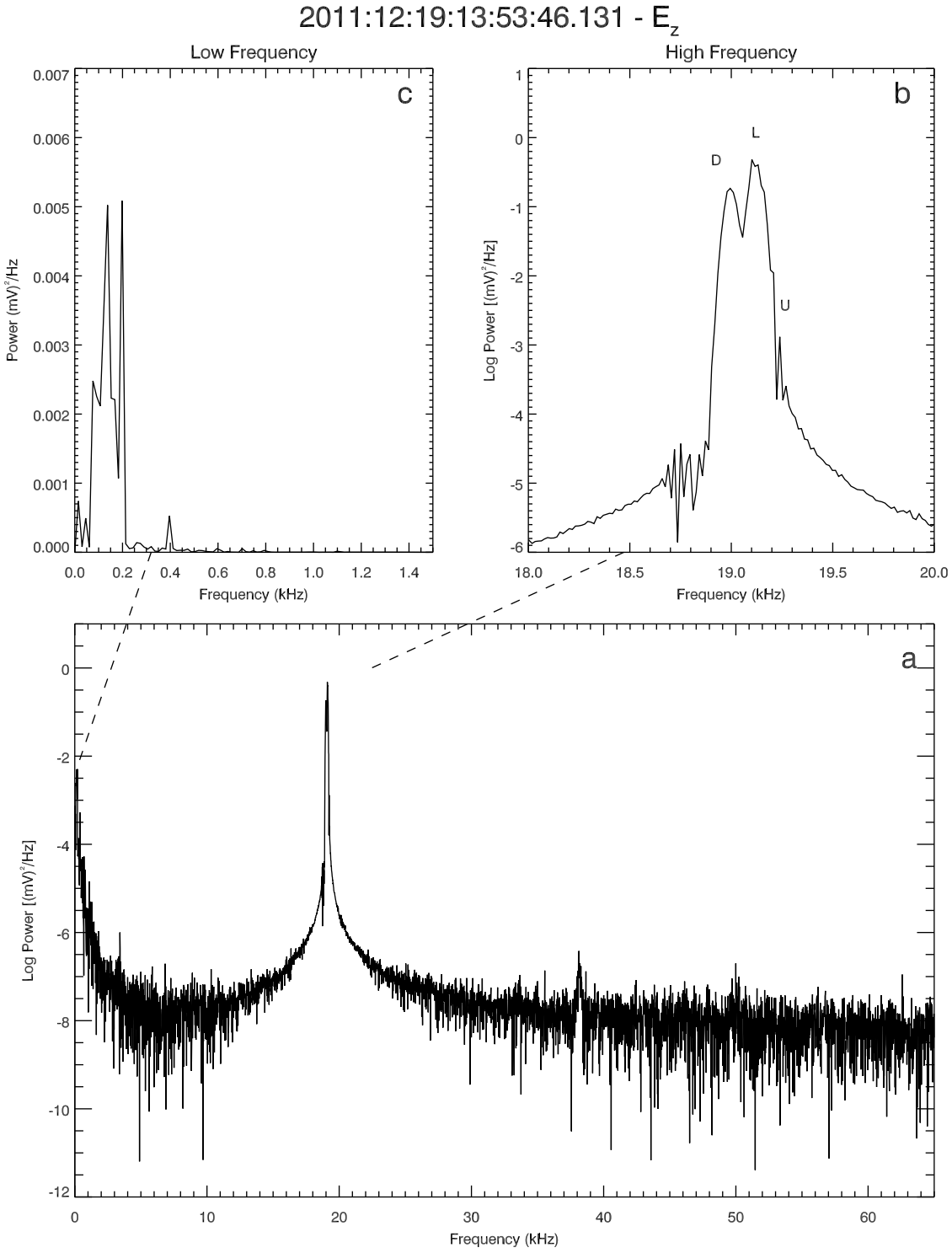

Figure 5. (a) The complete spectrum of the wave packet of Figure 4 from 0 to 65 kHz, (b) the narrow spectrum around $f \sim f_{pe} \sim 19.12$ kHz, where L, D, and U correspond to the beam excited Langmuir wave, down-shifted sideband at ~19 kHz, and up-shifted sideband at ~19.3 kHz, respectively, and (c) the low frequency spectrum: the enhancement below 200 Hz corresponds to ion-sound waves. The sideband emissions are probably due to nonlinear interactions between the beam excited Langmuir waves and ion sound waves.

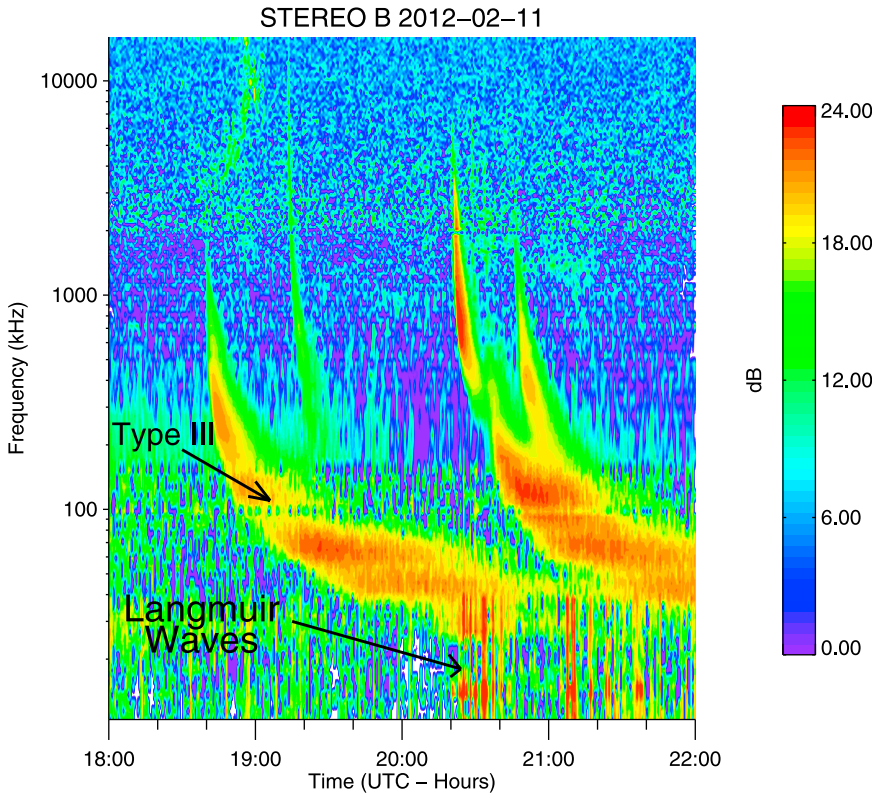

Figure 6. Dynamic spectrum of the second local type III radio burst (fast drifting emission from ~5 MHz down to ~20 kHz) and associated Langmuir waves (non-drifting emissions in the frequency interval 10–14 kHz).

can be estimated using the relation [*Lin et al.*, 1986; *Benz*, 2002]

$$\frac{\Delta k_L}{k_L} = \frac{\Delta v_b}{v_b}\frac{ln2}{2N}. \quad (7)$$

Here Δv_b is the velocity dispersion of the beam, $N \simeq \ln p$ is the number of linear growth times before the onset of MI, and p is the ratio of the peak electric field amplitude to the thermal background. We estimate that p is $\sim 10^4$ for all four events. It is interesting to note that higher the N, the longer the time available for the linear beam-plasma instability to grow. For the events of the present study, we estimate the number of linear growth times N as ≥ 9 for $p \sim 10^4$. Thus, for $N \sim 9$ and $\Delta v_b \simeq 0.1 v_b$, we obtain $\frac{\Delta k_L}{k_L} \simeq 3.9 \times 10^{-3}$. This value yields $\frac{\Delta\omega}{\omega_{pe}}$ as $\sim 2.2 \times 10^{-6}$, $\sim 2.5 \times 10^{-6}$, $\sim 1.4 \times 10^{-6}$ and $\sim 1.6 \times 10^{-6}$ for k_L of $\sim 1.3 \times 10^{-3}$ m^{-1}, $\sim 1 \times 10^{-3}$ m^{-1}, $\sim 1.1 \times 10^{-3}$ m^{-1} and $\sim 1.9 \times 10^{-3}$ m^{-1}, and λ_{De} of 10.3 m, 14.0 m, 9.8 m and 6.2 m, for the events I to IV, respectively. Thus the growth rates $\frac{\Gamma}{\omega_{pe}}$ are much larger than the bandwidths of beam-excited Langmuir wave packets $\frac{\Delta\omega}{\omega_{pe}}$. This suggests that the pump waves are monochromatic enough for excitation of supersonic MI. It is important to note that for the bandwidths of initial pump waves, one should not use the spectral widths from Figures 5b, 9b, 13b, and 17b since these are severely affected by the nonlinear effects.

[29] The peak intensity also decides whether the wave packet is a collapsing Langmuir soliton of the type described by *Zakharov* [1972] and *Nicholson et al.* [1978] or not. For the wave packet to be a collapsing soliton, it should satisfy the condition [*Thornhill and ter Haar*, 1978; *Gurnett et al.*, 1981]

$$\frac{W_L}{n_e T_e} \geq (\Delta k \lambda_{De})^2, \quad (8)$$

where $\Delta k = \frac{2\pi}{S}$ is the wave number characteristic of the envelope. Assuming that the wave packet is convected in the solar wind, we can convert the measured timescales τ of ~5.7 ms, ~7.9 ms, ~10 ms and ~7 ms into spatial scales S of $\sim 250\lambda_{De}$, $\sim 282\lambda_{De}$ $\sim 512\lambda_{De}$ and $\sim 355\lambda_{De}$ using the relation $S \sim \tau v_{sw}$ for v_{sw} of 450 km s^{-1}, 500 km s^{-1}, 500 km s^{-1} and 315 km s^{-1}, and λ_{De} of ~10.3 m, ~14.1 m, ~9.8 m and ~6.2 m, for the events I to IV, respectively. Thus, the observed $\frac{W_L}{n_e T_e}$ of $\sim 8.5 \times 10^{-4}$, $\sim 2.7 \times 10^{-3}$, $\sim 3.2 \times 10^{-3}$ and $\sim 1.3 \times 10^{-3}$ are greater than $(\Delta k \lambda_{De})^2$ of $\sim 6.3 \times 10^{-4}$, $\sim 5 \times 10^{-4}$, $\sim 1.5 \times 10^{-4}$ and $\sim 3.1 \times 10^{-4}$ obtained for the spatial scale S of $\sim 250\lambda_{De}$, $\sim 282\lambda_{De}$, $\sim 512\lambda_{De}$ and $\sim 355\lambda_{De}$ for events of Figures 4, 8, 12, and 16, respectively. This suggests that the observed wave packets are probably the Langmuir solitons collapsed to the spatial scales of a few hundred Debye lengths.

3.1. Spectral Characteristics

[30] As shown in Figure 1, MI, which is a four-wave interaction process excites a low frequency ion density perturbation of frequency and wave number (Ω, q). This perturbation can be either a freely propagating ion sound wave or a strongly damped quasi-mode. It can beat with two of the

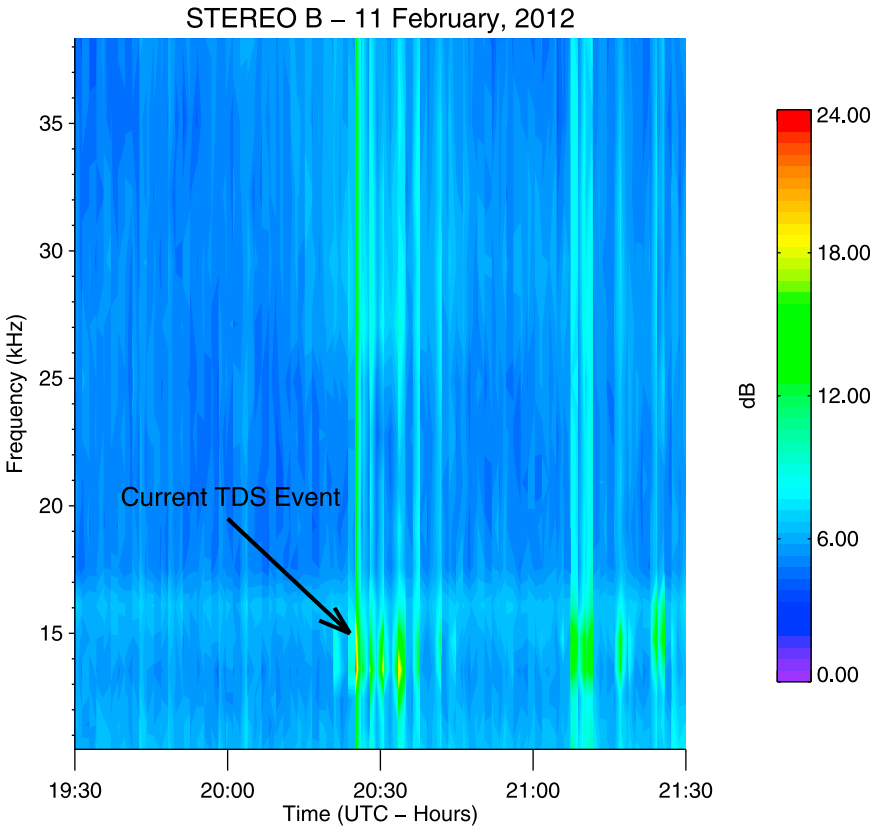

Figure 7. Frequency-time spectrogram of the Langmuir waves associated with the type III burst of February 11, 2012. The Langmuir wave emissions, which are very bursty show substantial frequency spreading. The arrow shows the Langmuir wave burst corresponding to the current TDS event.

initial pump waves with wave numbers, k_L and frequencies $f_L \sim f_{pe}$ (beam-excited Langmuir waves), and produce the down-shifted (Stokes) and up-shifted (anti-Stokes) sidebands with wave numbers and frequencies of $(\vec{k_L} - \vec{q})$ and $(f_L - \Omega)$, and $(\vec{k_L} + \vec{q})$ and $(f_L + \Omega)$, respectively. Thus, the Fourier spectrum resulting from such a four wave MI should contain the main emission peak at $f_L \sim f_{pe}$ together with two sidebands at $(f_L - \Omega)$ and $(f_L + \Omega)$, and a low frequency component. In the present case, the spectral peaks seen in Figures 5b, 9b, 13b, and 17b probably correspond to the down-shifted sideband (Stokes (D)), beam-excited Langmuir (L) and up-shifted sideband (anti-Stokes (U)) modes, respectively, and the low frequency spectral enhancements seen in Figures 5c, 9c, 13c, and 17c correspond to ion acoustic waves. This suggests that the observed spectral structures of the wave packets show one-to-one correspondence with the characteristic spectral signatures of the MI.

[31] The requirement for the observed spectral components to be associated with MI is that they should satisfy the frequency, wave number and phase matching conditions:

$$2f_L = f_D + f_U \tag{9}$$

$$2k_L = k_D + k_U \tag{10}$$

$$2\phi_L = \phi_D + \phi_U, \tag{11}$$

where, the subscripts L, D and U correspond to the beam-excited Langmuir, down-shifted sideband (Stokes) and up-shifted sideband (anti-Stokes) modes, respectively.

[32] In order for the frequency matching condition to be satisfied, the down-shifted (Stokes) and up-shifted (anti-Stokes) sidebands should be symmetric with respect to the beam-excited Langmuir wave, and their frequency shifts $\Delta f = f - f_{pe}$ should be in the frequency ranges of the respective low frequency enhancements.

[33] For December 19, 2011 event (Figure 5b), the frequency shifts of the down-shifted and up-shifted sidebands are reasonably symmetric with respect to the Langmuir wave pump, being ~120 Hz and ~180 Hz, respectively. These frequency shifts are in good agreement with the observed frequencies of ion sound waves of <200 Hz (Figure 5c). For February 11, 2012 event (Figure 9b), the frequency shifts of the down-shifted and up-shifted sidebands with respect to Langmuir waves are ~220 Hz and ~250 Hz, respectively, which are in agreement with the observed frequencies of ion sound waves of ~250 Hz. For July 18, 2009 event (Figure 13), the frequency shifts of the D and U modes (Figure 13b) are ~250 Hz and ~220 Hz, which are again in good agreement with the observed frequencies <250 Hz of the low frequency enhancement as seen in Figure 13c. The U mode in this case is weaker than the D mode, probably because it suffers higher damping rate in comparison with that of the D mode.

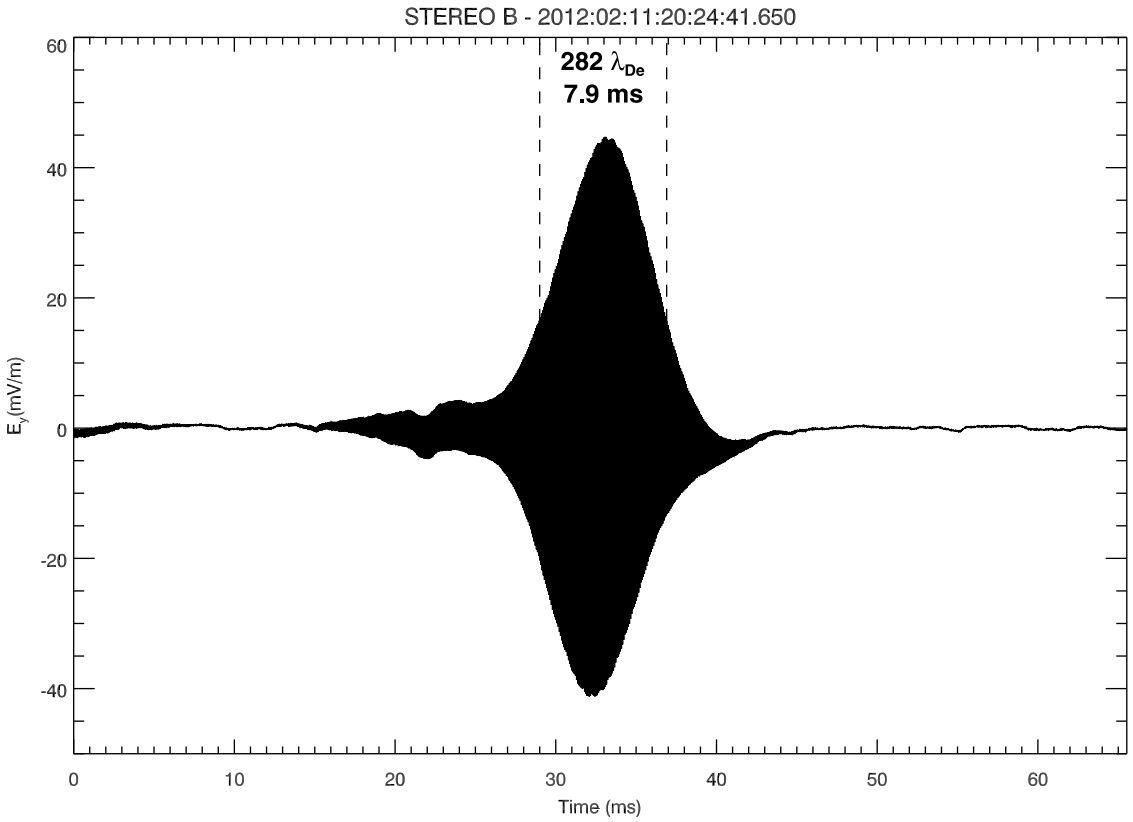

Figure 8. One of the most intense Langmuir wave packets captured by the Time Domain Sampler (TDS) during the type III event of Figure 6. The $\frac{1}{e}$ power duration of 7.9 ms of this event is equivalent to the spatial scale of $282\lambda_{De}$. The peak intensity E_L of this wave packet is ~44.7 mVm^{-1}.

[34] In the case of TDS event of December 5, 2006, the spectral peak at ~31.6 kHz in Figure 17b corresponds to the beam-excited Langmuir wave, the spectral peaks below this frequency correspond to Stokes modes propagating anti-parallel to the beam, and the spectral peaks at frequencies higher than 31.6 kHz correspond to anti-Stokes modes propagating parallel to the beam. The connection between the structure in the spectrum of this event and the MI is as follows. The MI excites low frequency ion density perturbations of frequency and wave number (Ω, q), which can beat with two of the initial beam excited Langmuir waves, producing high frequency sidebands with wave numbers $\vec{k_L} - \vec{q}$ (Stokes mode) and $\vec{k_L} + \vec{q}$ (anti-Stokes mode). These Stokes and anti-Stokes modes can again couple to the pump wave and regenerate the initial low frequency density perturbation at $\vec{q}$; they can also couple to each other to generate another low frequency density perturbation at $2\vec{q}$. This new density perturbation can beat with the pump to produce another pair of Stokes and anti-Stokes waves at $\vec{k_L} \pm 2\vec{q}$ which beat together to produce another density perturbation at $4\vec{q}$, which, in turn, will also generate new Stokes and anti-Stokes waves. A hierarchy of low frequency density perturbations together with higher order sidebands are thus generated. This process of producing higher order sidebands can proceed as long as the level of ion density fluctuations are above the thermal level. The frequency shifts of all the Stokes and anti-Stokes modes are in the frequency range of the low frequency enhancement seen in Figure 17c.

[35] We can estimate the wave numbers of the down-shifted and up-shifted sidebands and examine whether they satisfy the required matching condition as follows. The wave numbers k of the sidebands can be estimated using the expression for the Doppler shift:

$$\Delta f = \frac{v_{sw}}{2\pi\lambda_{De}}(k\lambda_{De})\cos\theta, \tag{12}$$

where θ is the angle between $\vec{k}$ and $\vec{v_{sw}}$, i.e., $\theta = 0$ and $\theta = \pi$ correspond to the anti-Stokes and Stokes modes propagating away from and toward the Sun, respectively. The pump Langmuir waves, the sidebands and ion sound waves should satisfy the conservation relation

$$\vec{k} = \vec{k_L} \pm \vec{q}, \tag{13}$$

where the plus and minus signs correspond to anti-Stokes and Stokes modes, respectively. Since the wave numbers of the pump waves k_L are usually much smaller than q, the $|\vec{q}|$ should be $\simeq \left|\vec{k}\right|$.

[36] In the case of TDS event of Figure 4, the frequency shifts of the D and U modes of ~120 Hz and ~180 Hz as seen in Figure 5b are <200 Hz, which is the frequency range of the low frequency enhancement seen in Figure 5c.

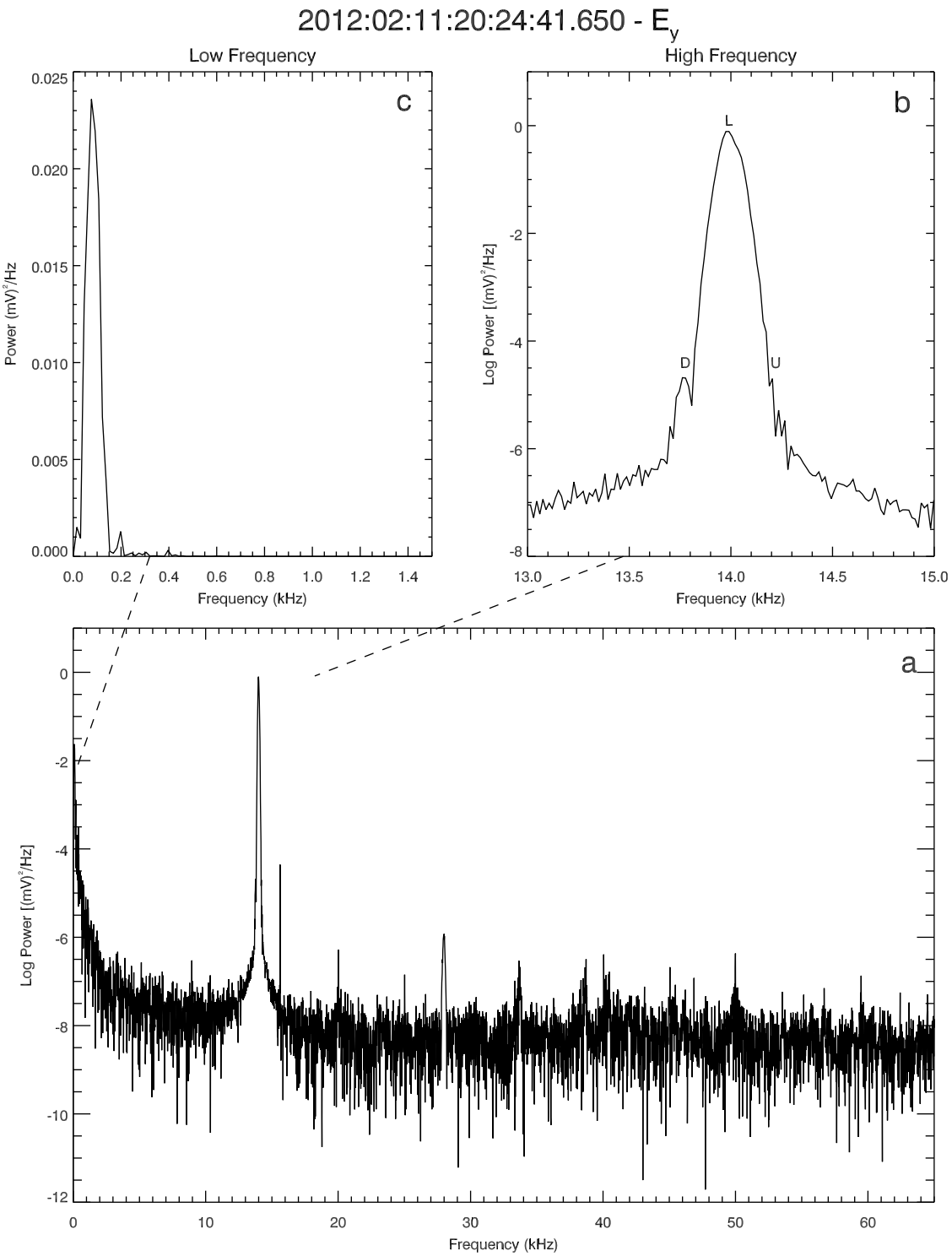

Figure 9. (a) The complete spectrum of the wave packet of Figure 8 from 0 to 65 kHz, where the primary peak at ∼14 kHz corresponds to beam excited Langmuir wave, (b) the narrow logarithmic spectrum around $f \sim f_{pe} \sim 14$ kHz, where the spectral peaks L, D, and U correspond to the beam excited Langmuir wave, down-shifted sideband ∼13.78 kHz, and up-shifted sideband ∼14.25 kHz, respectively, and (c) the low frequency linear spectrum: the enhancement below 250 Hz corresponds to ion-sound waves. The nonlinear interactions between the beam-excited Langmuir waves and the ion sound waves observed are probably responsible for the sideband emissions.

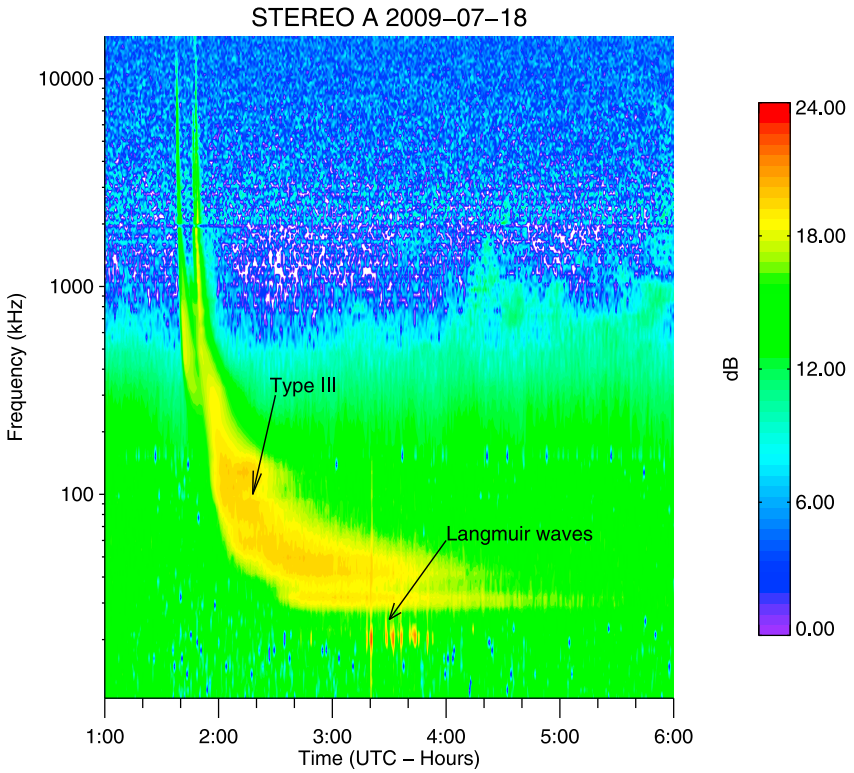

Figure 10. Dynamic spectrum of the third local type III radio burst (fast drifting emission from ~5 MHz down to ~20 kHz) and associated Langmuir waves (non-drifting emissions in the frequency interval 19–22 kHz).

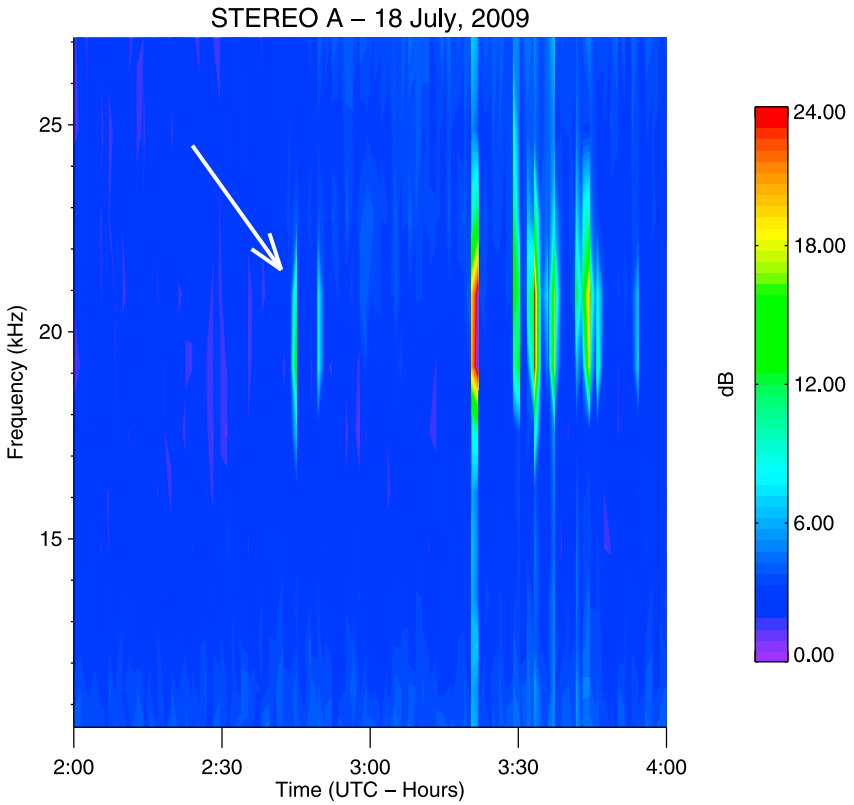

Figure 11. Frequency-time spectrogram of the Langmuir waves associated with type III burst of July 18, 2009. The arrow shows the Langmuir wave burst corresponding to the current TDS event.

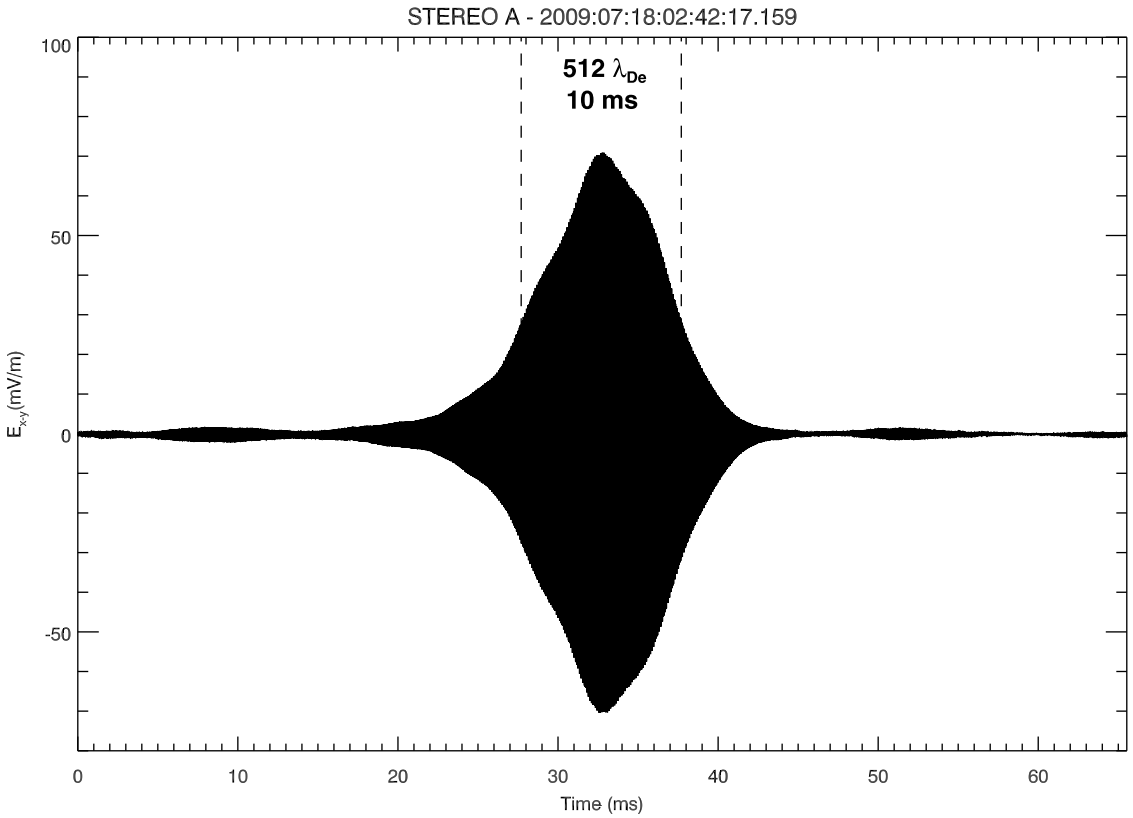

Figure 12. One of the most intense Langmuir wave packets captured by the Time Domain Sampler (TDS) during the type III event of Figure 10. The $\frac{1}{e}$ power duration of 10 ms of this event is equivalent to the spatial scale of $512\lambda_{De}$. The peak intensity E_L of this event is $\sim$70.9 mVm^{-1}.

Substituting these measured values $\Delta f \sim$ 120 Hz and $\Delta f =$ 180 Hz in equation (12), we estimate $k\lambda_{De}$ as ~ -0.017 and $\sim$0.026, for the Stokes and anti-Stokes modes with $\theta = 180°$ and $\theta = 0°$, respectively. These values indicate that the pump Langmuir waves with $k_L\lambda_{De} \sim 0.014$ are very efficiently converted into those of forward and backward propagating daughter Langmuir waves with large wave numbers. As far as the ion sound waves seen in Figure 5c are concerned, since their phase velocities are usually well below v_{sw}, their frequency spectrum in the spacecraft frame of reference is solely determined by the Doppler shifts. Thus, the upper limit of the wave numbers of these waves can be estimated as $q = \frac{2\pi\Omega}{v_{sw}} \simeq 2.8 \times 10^{-3}$ m^{-1} and $q\lambda_{De} \simeq 0.029$ for $\Omega =$ 200 Hz and $v_{sw} = 450$ km s^{-1}. Thus, the wave numbers of the observed low frequency waves are comparable to those of the sideband emissions.

[37] In the case of TDS event of Figure 8, the frequency shifts of the D and U modes $\sim$220 Hz and $\sim$250 Hz are in agreement with the observed frequencies of ion sound waves of $\sim$250 Hz. Substituting these measured values $\Delta f \sim$ 220 Hz and $\Delta f =$ 250 Hz in equation (12), we can estimate $k\lambda_{De}$ as ~ -0.039 and $\sim$0.044, for the Stokes and anti-Stokes modes, respectively, and compare them with $k_L\lambda_{De} \sim 0.015$. The upper limit of the wave numbers of the ion sound waves of Figure 9c can be estimated as $q = \frac{2\pi\Omega}{v_{sw}} \simeq 3.1 \times 10^{-3}$ m^{-1} and $q\lambda_{De} \simeq 0.044$ for $\Omega = 250$ Hz and $v_{sw} = 500$ km s^{-1}. Thus, the wave numbers of the observed low frequency waves are comparable to those of the sideband emissions.

[38] In the case of July 18, 2009 event (Figure 12), for the Stokes and anti-Stokes modes with $\theta = 180°$ and $\theta = 0°$, we can plug the measured values of $\Delta f \sim$ 250 Hz and 220 Hz in equation (12) and estimate $k\lambda_{De}$ as ~ -0.031 and $\sim$0.027, respectively. These values of $k\lambda_{De}$ are much higher than $k_L\lambda_{De} \sim 0.015$. As far as the ion sound waves seen in Figure 13c are concerned, the upper limit of their wave numbers are estimated as $q = \frac{2\pi\Omega}{v_{sw}} \simeq 3.1 \times 10^{-3}$ m^{-1} and $q\lambda_{De} \simeq 0.031$ for $\Omega = 250$ Hz and $v_{sw} = 500$ km s^{-1}. Thus, the wave numbers of the observed low frequency waves are comparable to those of the sideband emissions, which indicates that the observed low frequency waves are probably involved in parametric interaction with the Langmuir waves.

[39] In the case of Dec 5, 2006 event (Figure 16), we can estimate $k_L\lambda_{De} \sim 1.2 \times 10^{-2}$ for k_L is $\sim 1.9 \times 10^{-3}$ m^{-1} and $\lambda_{De} \sim 6.2$ m. Plugging the maximum measured Δf of 200 Hz in equation (12), we estimate that the wave numbers k of the anti-Stokes and Stokes modes should be as large as $\sim 2k_L$. Thus, the spectral observations of Langmuir wave packets show that the beam excited Langmuir waves presented in Figure 16 with $k_L\lambda_{De}$ of $\sim$0.012 are very efficiently converted into those of the forward and backward propagating daughter waves with large wave numbers up to $k\lambda_{De} \sim 0.025$. As far as the wave numbers of low frequency waves (Figure 17c) are concerned, we can estimate $q = \frac{2\pi\Omega}{v_{sw}} \simeq$

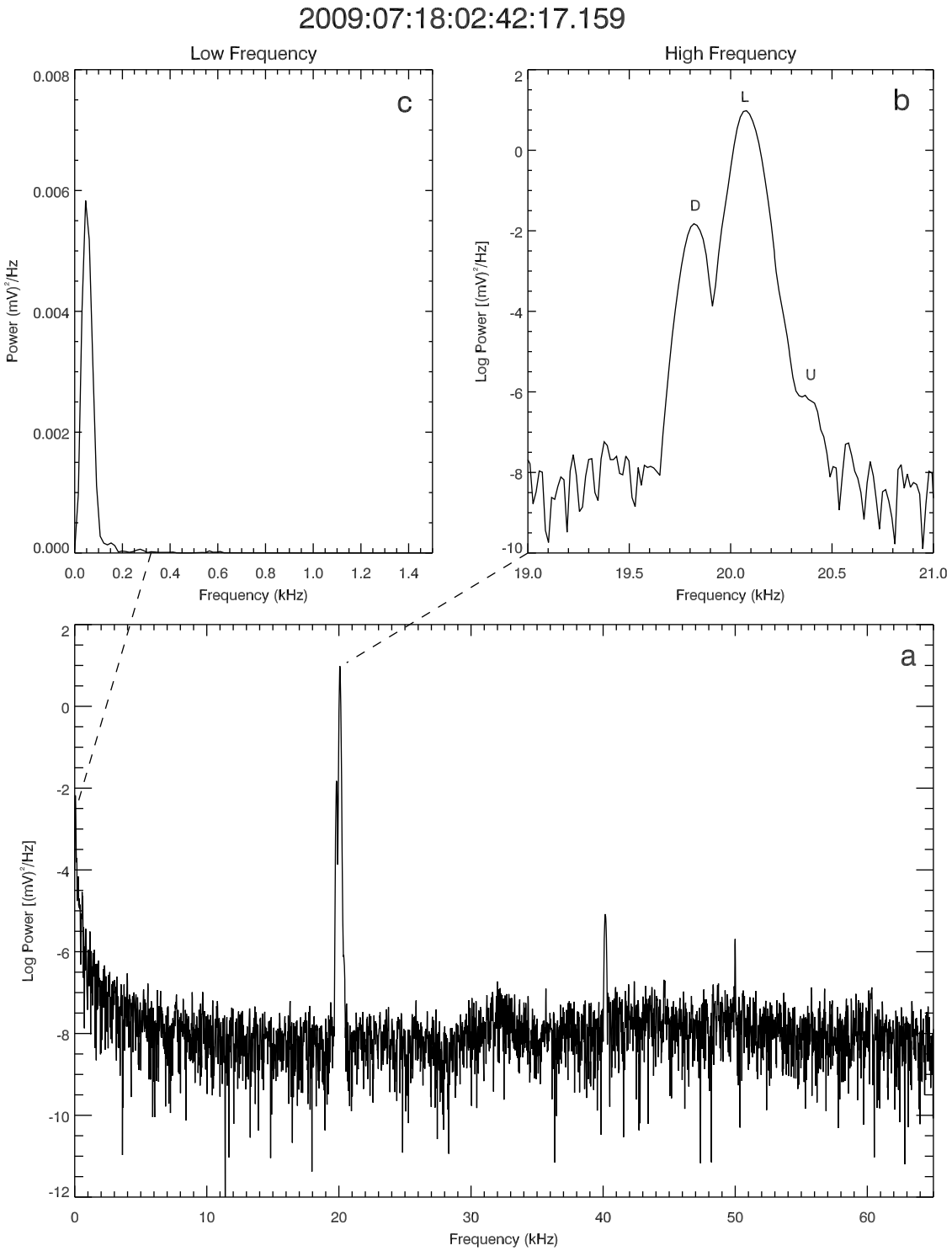

Figure 13. (a) The complete spectrum of the wave packet of Figure 12 from 0 to 65 kHz, where the dominant spectral peak at ∼20.1 kHz corresponds to the Langmuir wave excited by the electron beam at local electron plasma frequency, f_{pe}, (b) the narrow spectrum around the main Langmuir wave peak at $f \sim f_{pe} \sim$ 20.1 kHz, where L, D, and U correspond to the beam excited Langmuir wave, down-shifted sideband at ∼19.85 kHz, and up-shifted sideband peak at ∼20.32 kHz, respectively, and (c) the low frequency spectrum: the enhancement below 250 Hz probably corresponds to ion-sound waves.

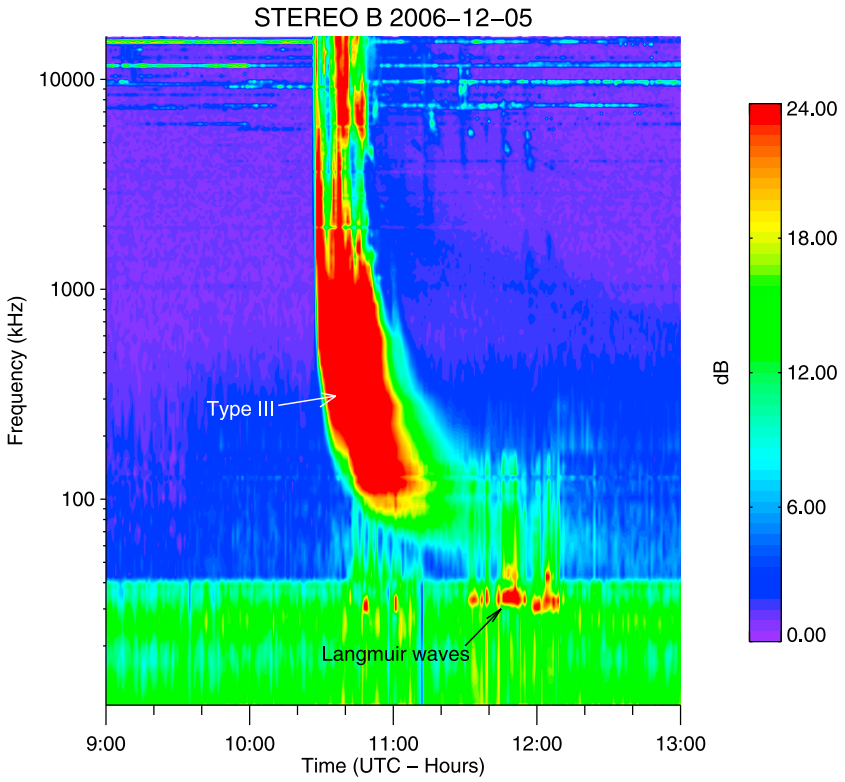

Figure 14. Dynamic spectrum of the fourth local type III radio burst (fast drifting emission from ~5 MHz down to ~32 kHz) and associated Langmuir waves (non-drifting emissions in the frequency interval 28–32 kHz).

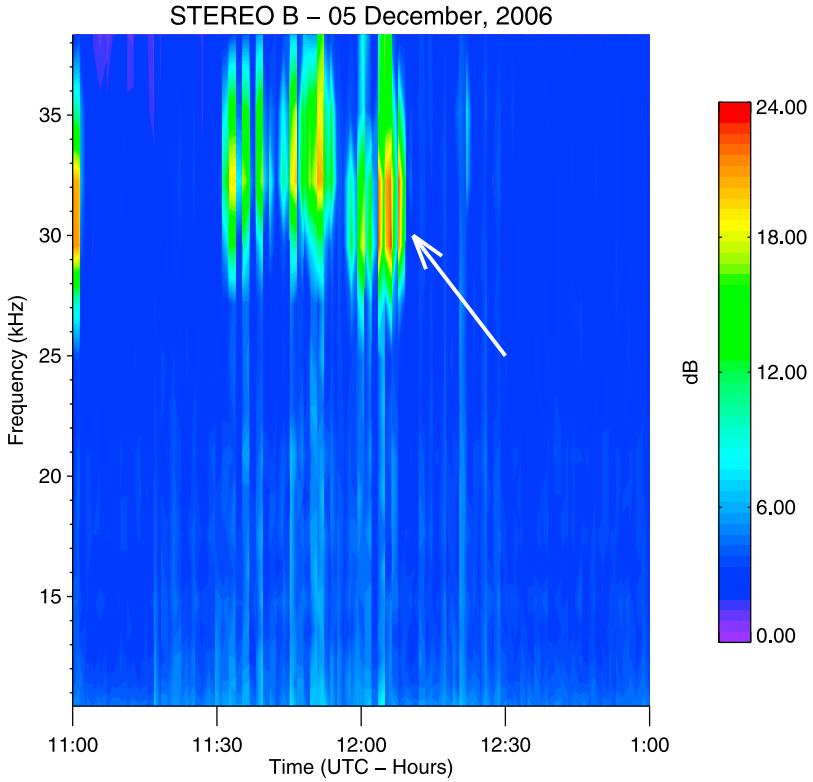

Figure 15. Frequency-time spectrogram of the Langmuir waves associated with the type III burst of December 5, 2006. The Langmuir wave emissions are very clumpy and show substantial frequency spreading. The arrow shows the location of the current TDS event.

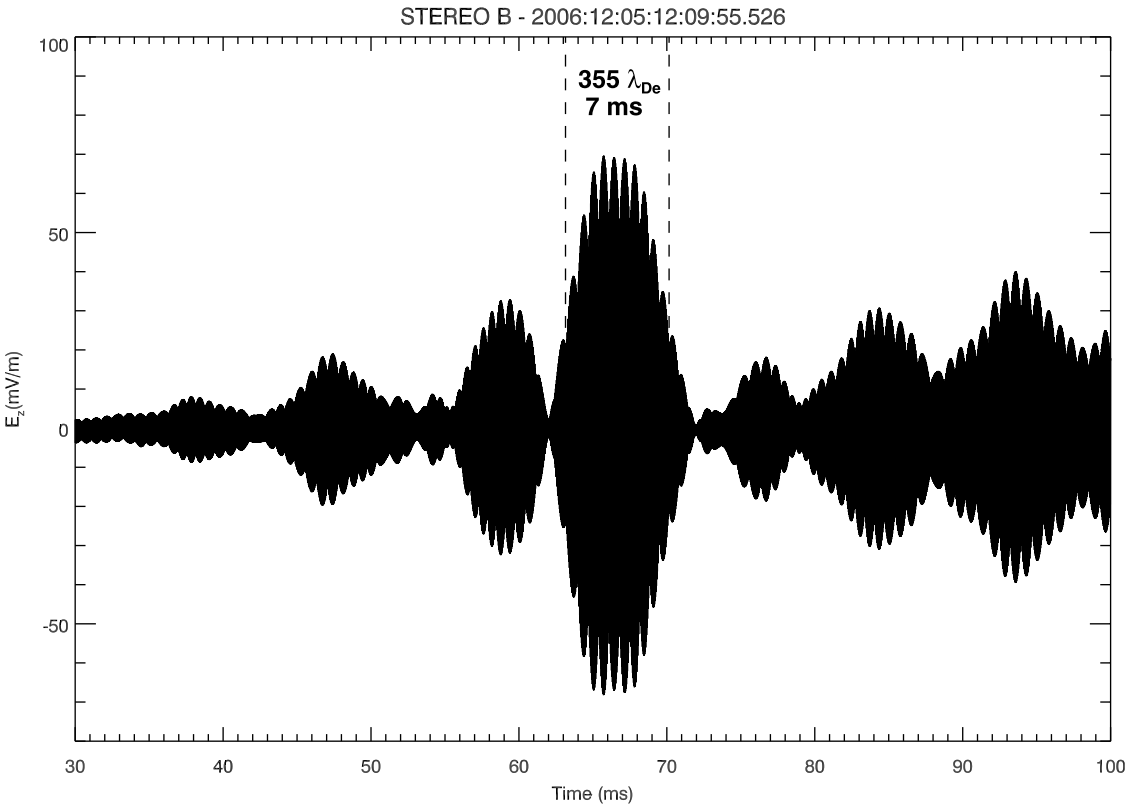

Figure 16. One of the most intense waveforms of Langmuir waves observed by the Time Domain Sampler (TDS) during the type III event of December 5, 2006. The $\frac{1}{e}$ power duration of 7 ms is equivalent to the spatial scale of $355\lambda_{De}$. The peak intensity E_L of this wave packet is $\sim$69.7 mVm^{-1}.

4×10^{-3} m^{-1} and $q\lambda_{De} \simeq 0.025$ for Ω = 200 Hz and v_{sw} = 315 km s^{-1}. These wave numbers of low frequency waves are comparable to those of sideband waves.

[40] Thus, the sidebands and low frequency enhancements contained in the spectra of TDS events of Figures 4, 8, 12, and 16 probably correspond to the daughter waves excited by the MI.

3.2. Trispectral Analysis

[41] The conventional spectral analysis does not yield complete information about the nonlinear processes from the waveform data. To extract the phase coherence amongst spectral components of the wave packets, the higher order spectral analysis techniques, namely, the bispectral and trispectral analysis techniques should be used. The bi-spectral analysis can extract the nonlinear characteristics between three spectral components with frequency sum and difference [*Kim and Powers*, 1979]. Since bi-spectral analysis is related to the skewness of a signal, it can detect only the asymmetric non-linearities, such as the electrostatic decay [*Henri et al.*, 2009; *Balikhin et al.*, 2001; *Walker et al.*, 2002, 2003] and harmonic generation [*Bale et al.*, 1996]. The amplitude of the bispectrum at the bifrequency (F_k, F_l) measures the amount of coupling between the frequencies, F_k, F_l and F_{k+l}. The trispectral analysis, on the other hand, is used to demonstrate the occurrence of cubic nonlinear interactions in the system. The tricoherence spectra can isolate the individual cubic interactions between quartets of spectral components, especially those associated with oscillations at the power spectral primary peak frequency and its sidebands, as well as their combination tones.

[42] A cumulant based trispectral method has been developed and applied to synthetic [*Kravtchenko-Berejnoi et al.*, 1995a, 1995b; *Lefeuvre et al.*, 1995] and simulated data [*Soucek et al.*, 2003]. The expression for the trispectrum can be written as [*Kravtchenko-Berejnoi et al.*, 1995a]

$$T(k,l,p) = E\left[X_k X_l X_p^* X_q^*\right] - N(k,l,p,q), \qquad (14)$$

where X_k, X_l, X_p and X_q are the complex Fourier components of the signal at frequencies F_k, F_l, F_p and $F_q = F_k + F_l - F_p$, and $N(k, l, p, q) = E[X_k X_l]E[X_p^* X_q^*] + E[X_k X_p^*]E[X_l X_q^*] + E[X_k X_q^*]E[X_l X_p^*]$. Here $E[]$ is the expectation operator. In the present case, the subscripts k and l refer to beam excited Langmuir waves, and p and q refer to down-shifted (Stokes) and up-shifted (anti-Stokes)sidebands, respectively.

[43] The normalized trispectrum is usually referred to as the tricoherence. It is more useful because it eliminates the dependence of trispectrum on the amplitudes of the signals. The tricoherence quantifies the phase coherence amongst the spectral components of the wave packet, i.e., it quantifies the fraction of the total product of powers at the frequency quartet, (F_k, F_l, F_p, $F_q = F_k + F_p - F_l$), that is owing to cubicly phase-coupled modes. The expression for the square

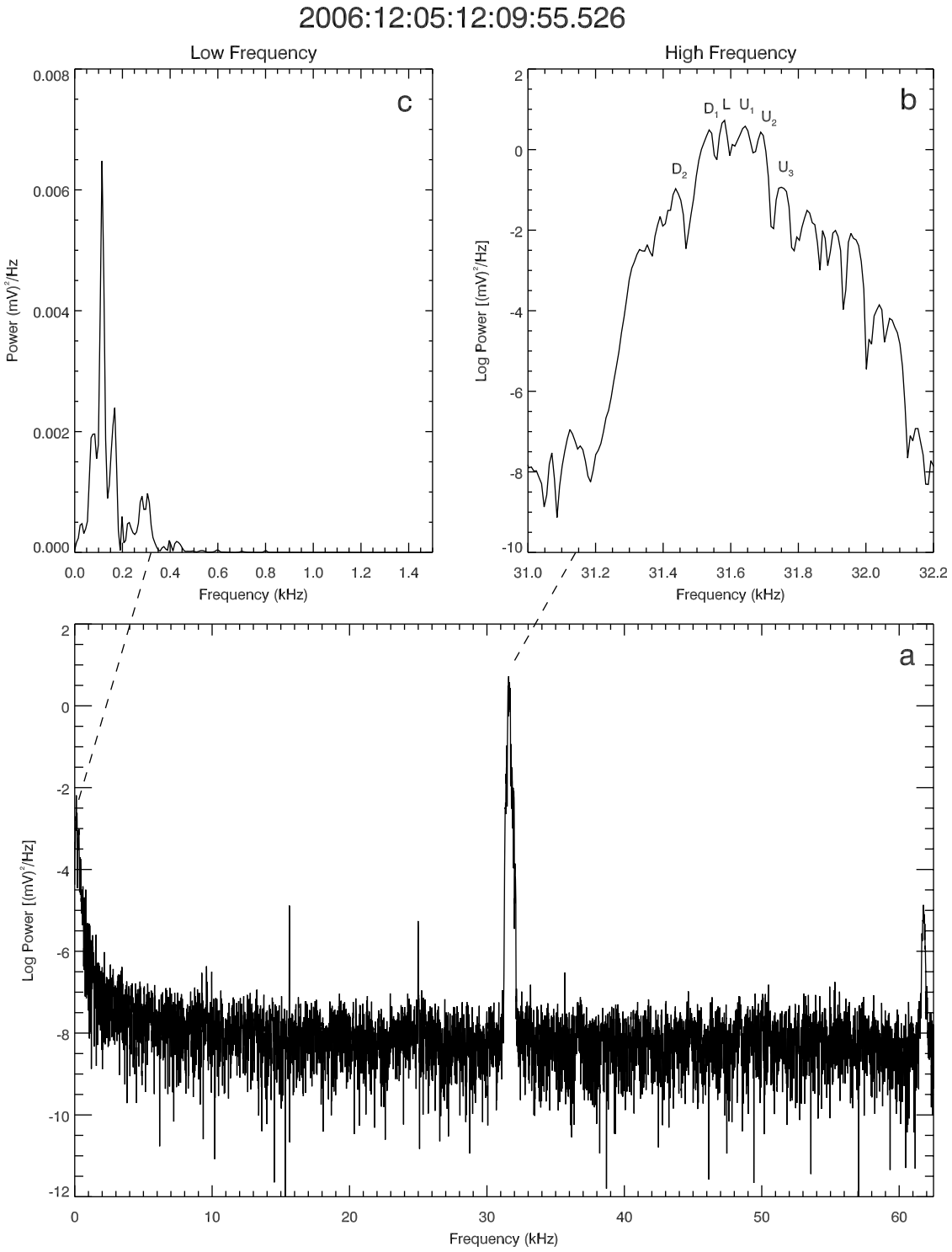

Figure 17. (a) The complete spectrum of the wave packet of Figure 16 from 0 to 65 kHz, where the dominant spectral peak at ~31.6 kHz corresponds to the beam excited Langmuir wave, (b) the narrow spectrum around $f \sim f_{pe} \sim 31.6$ kHz, where the main peak is denoted as L, the down-shifted (Stokes) sidebands are denoted as D_1 and D_2, and up-shifted (anti-Stokes) sidebands are denoted as U_1, U_2 and U_3. (c) The low frequency spectrum, which shows a clear enhancement below 200 Hz corresponding to ion-sound waves.

Table 1. Relevant Parameters

Parameters	19/12/2011	11/2/2012	18/7/2009	5/12/2006
Electron Density, n_e m^{-3}	4.5×10^6	2.4×10^6	5×10^6	1.2×10^7
Solar wind velocity, v_{sw} km s^{-1}	450	500	500	315
Electron Temperature, T_e(K)	10^5	10^5	10^5	10^5
Debye length, λ_{De} (m)	10.3	14	9.8	6.2
Electron plasma frequency, f_{pe} (kHz)	19.12	14	20.1	31.6
Electron Thermal velocity, v_{Te} (ms^{-1})	1.23×10^6	1.23×10^6	1.23×10^6	1.23×10^6
Beam velocity, v_b	$0.3c$	$0.28c$	$0.37c$	$0.35c$
Beam width, $\frac{\Delta v_b}{v_b}$	~0.1–0.2	~0.1–0.2	~0.1–0.2	~0.1–0.2
Beam resonant wave number, k_L (m^{-1})	1.3×10^{-3}	1×10^{-3}	1.1×10^{-3}	1.9×10^{-3}
Peak wave amplitude, E_L (mVm^{-1})	34.6	44.7	70.9	69.7
Normalized energy density, $\frac{W_L}{n_e T_e}$	8.5×10^{-4}	2.6×10^{-3}	3.2×10^{-3}	1.3×10^{-3}
$\frac{1}{e}$-level duration (ms)	5.7	7.9	10	7
$\frac{1}{e}$-level size (λ_{De})	250	282	512	355
Peak tricoherence	0.35	0.58	0.32	0.32

tricoherence can be written as [*Kravtchenko-Berejnoi et al.*, 1995a]:

$$t^2(k,l,p) = \frac{|T(k,l,p)|^2}{\left(E\left[\left|X_k X_l X_p^* X_q^*\right|\right] + |N(k,l,p,q)|\right)^2}. \quad (15)$$

A unit value of the tricoherence indicates perfect coupling, a zero value indicates no coupling, and any value between zero and one indicates partial coupling.

[44] The tricoherence is zero for a Gaussian process. Even for a Gaussian process, due to statistical fluctuations, the estimate of the tricoherence from a finite data record will not be zero. Therefore, the method of periodograms is usually used to estimate the trispectrum and tricoherence. This method involves the division of the data record into M segments; an appropriate window is applied to each segment to reduce leakage; the trispectrum as well as tricoherence are computed for each segment by using the DFT; finally, the trispectrum and tricoherence are averaged across segments to reduce the variance of the estimator.

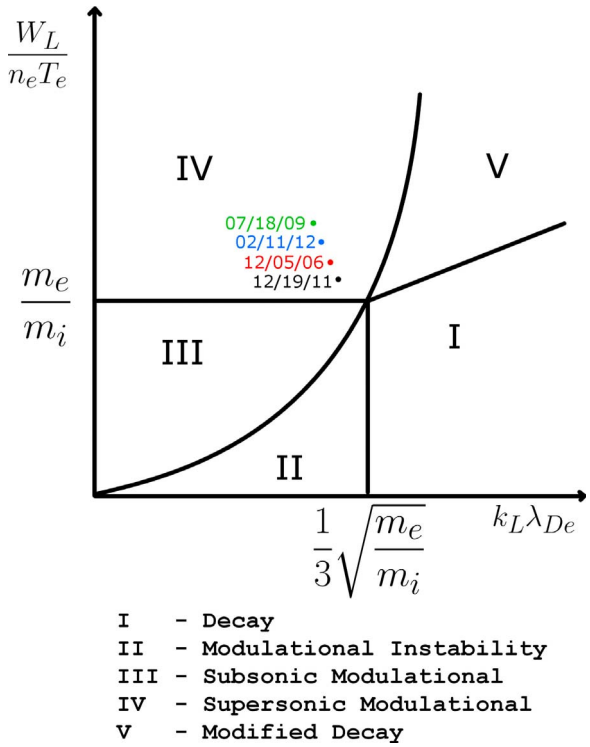

Figure 18. Different regimes of Langmuir turbulence.

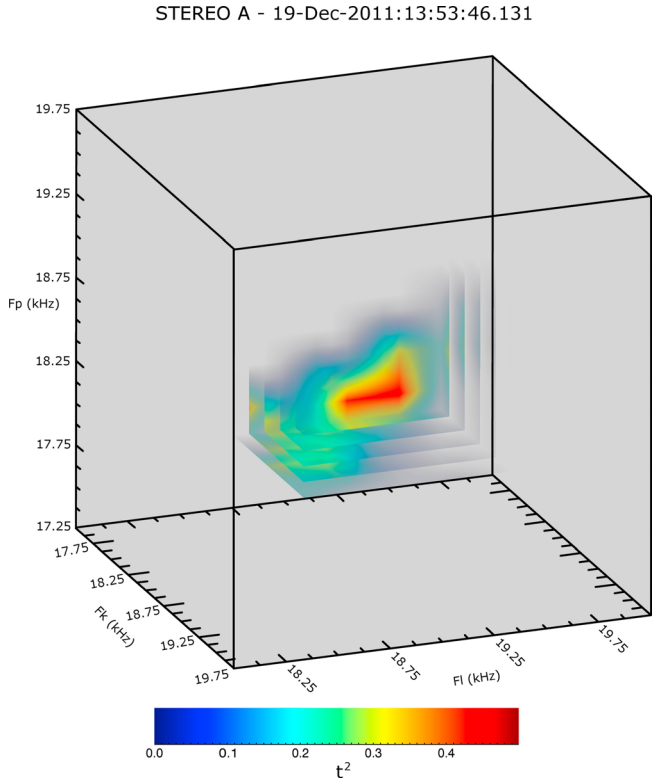

Figure 19. The three dimensional representation of the tricoherence spectrum $t^2(F_k, F_l, F_p)$ of the TDS event of 2011 December 19 (Figure 4). The tricoherence t^2 exhibits peak value of ~0.35 at (~19.25, ~19, ~18.75) kHz, which quantifies the phase relation $2\phi_L = \phi_D + \phi_U$, where ϕ_L, ϕ_D and ϕ_U are the phases of the beam-excited Langmuir wave at ~19.12 kHz, Stokes (~19 kHz) and anti-Stokes (~19.3 kHz) modes, respectively.

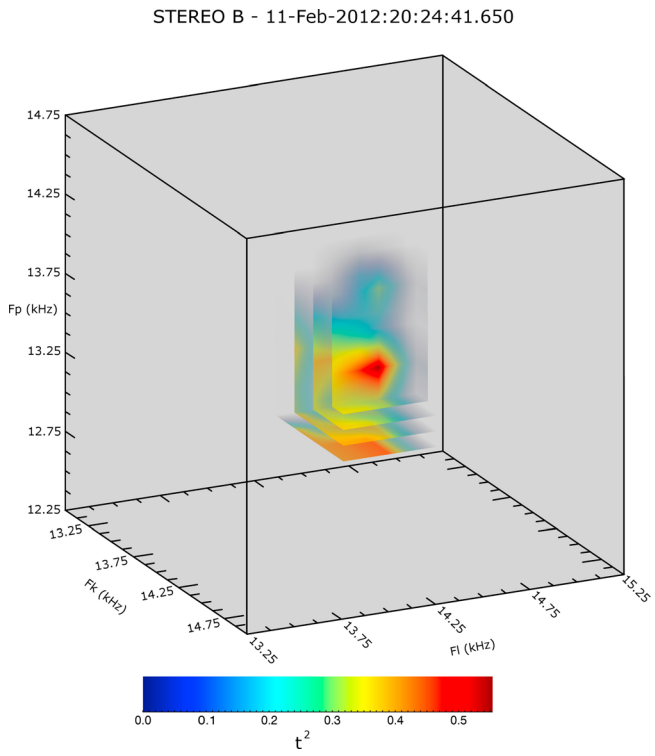

Figure 20. The 3-D representation of the tricoherence spectrum $t^2(F_k, F_l, F_p)$ of the TDS event of Figure 8 (2012 February 11). The peak tricoherence of ~0.58 at frequency quartet ($F_k \sim 14.5$, $F_l \sim 14.25$, $F_p \sim 13.75$, $F_q = F_k + F_p - F_l \sim 14.125$) kHz quantifies the phase coherence between two beam excited Langmuir waves and, a down-shifted and an up-shifted sidebands.

[45] As seen from equation (14), the trispectrum estimator is symmetric with respect to permutations of its arguments F_k, F_l and F_p. The principal domain for the interaction of the type $F_k + F_l = F_p + F_q$ is determined as [*Kravtchenko-Berejnoi et al.*, 1995a] $0 \le F_k \le f_N$, $0 \le F_l \le F_k$, $0 \le F_p \le F_l$, and $F_p \le F_k + F_l - F_p \le f_N$, where f_N is the Nyquist frequency.

[46] *Thejappa et al.* [2012a] reported the observations of a highly localized Langmuir wave packet captured by the TDS during one of the local type III events. This wave packet was characterized by a short duration of ~3 ms, peak intensity exceeding the threshold for the OTSI as well as spatial collapse, and the spectrum, containing the signatures of OTSI, namely, an intense peak corresponding to beam-resonant Langmuir wave, two sidebands corresponding to down-shifted and up-shifted daughter Langmuir waves, and a low frequency enhancement corresponding to daughter ion sound waves; the frequencies and wave numbers of these spectral components satisfied the resonance conditions of OTSI. Since the spectral methods are phase blind, *Thejappa et al.* [2012b] had developed cumulant based trispectral analysis tools to extract the phase information. Using those tools, these authors have clearly demonstrated that the spectral components of the observed wave packet are coupled to each other with a high degree of phase coherency as expected of OTSI.

[47] In this study, we will use the trispectral analysis tools developed by *Thejappa et al.* [2012b] to extract the phase information amongst the spectral components of the wave packets of Figures 4, 8, 12, and 16. For this purpose, as expected of the periodogram method, we divide the time series into M = 16 segments with segment length N = 1000 (0.004 s). We apply the Hamming window for each segment, and calculate the tricoherence spectrum as a function of three frequencies F_k, F_l, and F_p.

[48] The true values of tricoherence are known to be zero for Gaussian noise [*Hasselman et al.*, 1963; *Nikias and Raghuveer*, 1987; *Dalle Molle and Hinich*, 1989]. The 90% significance level for estimate of tricoherence for Gaussian noise is given by [*Chandran et al.*, 1994]

$$t_G^2(k,l,p) = \frac{4.6}{2M}. \tag{16}$$

In the present case, for M = 16, we obtain $t_G^2 \sim 0.144$. Therefore, the tricoherence t^2 values above 0.144 are significant at the 90% significance level for M blocks of the data, i.e., for 2 M degrees of freedom. Although any tricoherence value between zero and one indicates a partial coupling of four waves, we consider only those values which are greater than 0.144 as significant.

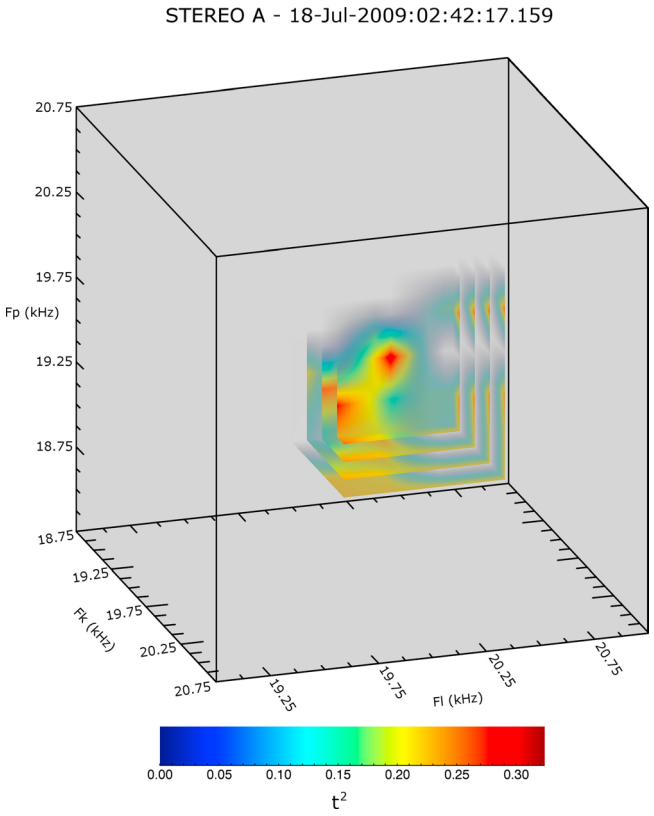

Figure 21. The 3-D tricoherence spectrum $t^2(F_k, F_l, F_p)$ of the TDS event of Figure 12 (2009 July 18). The peak tricoherence of ~0.32 at ($F_k \sim 20.25$ $F_l \sim 20$, $F_p \sim 19.75$, $F_q = F_k + F_p - F_l \sim 20$) kHz, quantifies the phase relation $2\phi_L = \phi_D + \phi_U$, where ϕ_L, ϕ_D and ϕ_U are the phases of the beam-excited Langmuir, Stokes and anti-Stokes modes, respectively.

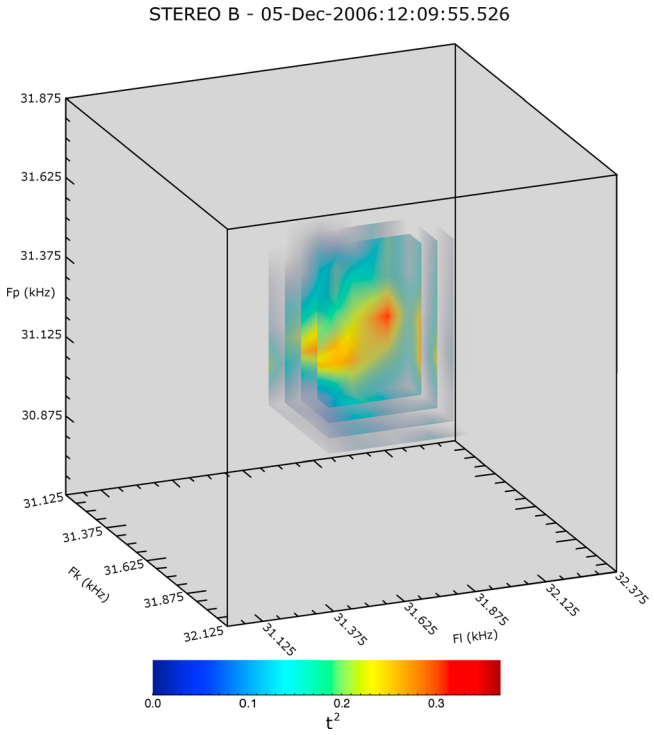

Figure 22. The 3-D tricoherence spectrum $t^2(F_k, F_l, F_p)$ of the TDS event of Figure 16 (2006 December 5). The peak coherence ~0.32 at the frequency quartet ($F_k \sim 31.5$, $F_l \sim 31.5$, $F_p \sim 31.25$, $F_q = F_k + F_l - F_p \sim 31.75$) kHz quantifies the phase relation $2\phi_L = \phi_D + \phi_U$, where ϕ_L, ϕ_D and ϕ_U are the phases of the beam-excited Langmuir, one of the Stokes and one of the anti-Stokes modes, respectively.

[49] Since it is difficult to visualize the tricoherence results in a 3-D space, usually one frequency is fixed and the tricoherence spectrum is displayed as a function of two frequencies. However, in the present study, we display the results in 3-D space, i.e., we display the tricoherence t^2 spectrum as a function of three frequencies, F_k, F_l and F_p. We restrict the frequencies to narrow relevant frequency ranges, centered around the frequency of the primary spectral peak, which in the present case is the local electron plasma frequency, f_{pe}. We construct the 3-D spectrum $t^2(\sim f_D \le F_k \le \sim f_U, \sim f_D \le F_l \le \sim f_U, \sim f_D \le F_p \le \sim f_U)$, where f_D and f_U correspond to the frequencies of down-shifted and up-shifted sidebands, respectively. Since the frequency resolution in the present case is ~250 Hz, the considered frequencies may not exactly coincide with the frequencies of the observed spectral peaks.

[50] In Figure 19, we present the 3-D tricoherence spectrum of the TDS event of 2011 December 19, constructed using the tricoherence t^2 values computed in the frequency ranges [19 kHz $\le F_l \le$ 19.75 kHz, 19 kHz $\le F_k \le$ 19.5 kHz, 18.75 kHz $\le F_p \le$ 19.25 kHz]. As seen from this 3-D representation, the tricoherence exhibits a spectral feature of finite volume in 3-D frequency space. However, The tricoherence attains a peak value of ~0.35 at (~19.25, ~19, ~18.75) kHz. This value of tricoherence, which is a statistically significant value by being greater than $t_G^2 \sim 0.144$ quantifies the phase relation $2\phi_L = \phi_D + \phi_U$, where ϕ_L, ϕ_D and ϕ_U are the phases of the beam-excited Langmuir wave at ~19.12 kHz, Stokes (~19 kHz) and anti-Stokes (~19.3 kHz) modes, respectively.

[51] For 2012 February 11 event, we present the 3-D tricoherence spectrum in Figure 20. This 3-D spectrum is constructed using the computed t^2 values in the frequency range [14.25 kHz $\le F_k \le$ 14.75 kHz, 14 kHz $\le F_l \le$ 14.25 kHz, 13.75 kHz $\le F_p \le$ 14.25 kHz]. Although, the tricoherence spectral feature has an extended shape in 3-D frequency space, it exhibits a peak of ~0.58 at (~14.5, ~14.25, ~13.75) kHz. This peak quantifies the phase coherence between two beam excited Langmuir waves at ~14 kHz and a down-shifted sideband at ~13.75 kHz and an up-shifted sideband at ~14.25 kHz.

[52] For the 2009 July 18 event, the 3-D tricoherence spectrum is presented in Figure 21. The tricoherences used in this figure are computed in the frequency ranges [20 kHz $\le F_k \le$ 20.75 kHz, 20 kHz $\le F_l \le$ 20.25 kHz, 19.75 kHz $\le F_p \le$ 20.25 kHz]. In this case, the t^2 attains a peak of ~0.32 at (~20.25, ~20, ~19.75) kHz. Again, since it is statistically significant, it quantifies the phase relation $2\phi_L = \phi_D + \phi_U$.

[53] In Figure 22, we present the 3-D tricoherence t^2 spectrum of the 2006 December 5 event. In this case, the tricoherence t^2 attains a peak of ~0.32. This is computed in the frequency range [31.625 kHz $\le F_k \le$ 31.875 kHz, 31.5 kHz $\le F_l \le$ 31.875 kHz, 31.25 kHz $\le F_p \le$ 31.75 kHz]. The corresponding frequency quartet is (~31.5, ~31.5, ~31.25, ~31.75) kHz. This tricoherence quantifies the phase relation $2\phi_L = \phi_D + \phi_U$.

[54] The results of tricoherence estimates can also be displayed as 2-D cross-sections at different frequencies. For example, for 2006 December 5 event, we present the cross sections of the tricoherence spectrum in Figure 23. The top panel shows the cross-section at $F_p = f_D = 31.25$ kHz, which shows a clear tricoherence spectral peak at (~31.5, ~31.5, ~31.25) kHz. The peak value of t^2 in this case is ~0.32. This value agrees with that of 3-D analysis. This peak tricoherence quantifies the phase relation $2\phi_L = \phi_D + \phi_U$, where ϕ_L, ϕ_D and ϕ_U are the phases of the beam-excited Langmuir wave (~31.5 kHz), one of the Stokes (~31.25 kHz) and one of the anti-Stokes (~31.75 kHz) modes, respectively, i.e., the frequency quartet in this case is (~31.5, ~31.5, ~31.25, ~31.75) kHz. The maximum tricoherence $t^2 \sim 0.32$ in this case is statistically significant.

[55] In the second panel, we present the cross-section of the tricoherence spectrum at $F_p = f_L = 31.50$ kHz. It shows two comparatively weaker spectral features, with peak values of ~0.21 at (~31.75 kHz, ~31.625 kHz, ~31.50 kHz) as well as at (~32, ~31.875, ~31.50) kHz. These relatively smaller tricoherence values reflect the weaker four wave interactions involving the sidebands themselves. In the bottom panel, we present the tricoherence cross-section at $F_p = f_U = 30.75$ kHz, which also shows a weak peak of ~0.21 at (~31.75, ~31.875, ~32.125) kHz. This again reflects the four wave interactions involving the sidebands themselves. However, the tricoherence spectral peak $t^2 \sim 0.32$ (top panel) is more significant in the statistical sense. Therefore, the dominant four wave interaction in this case is $2f_L \rightarrow f_D + f_U$. One should note that, the structure in the spectrum of this TDS event as seen in Figure 17b with multiple sidebands and the tricoherence peaks in the second and third panels indicate that the four wave interactions between the sidebands also can be possible.

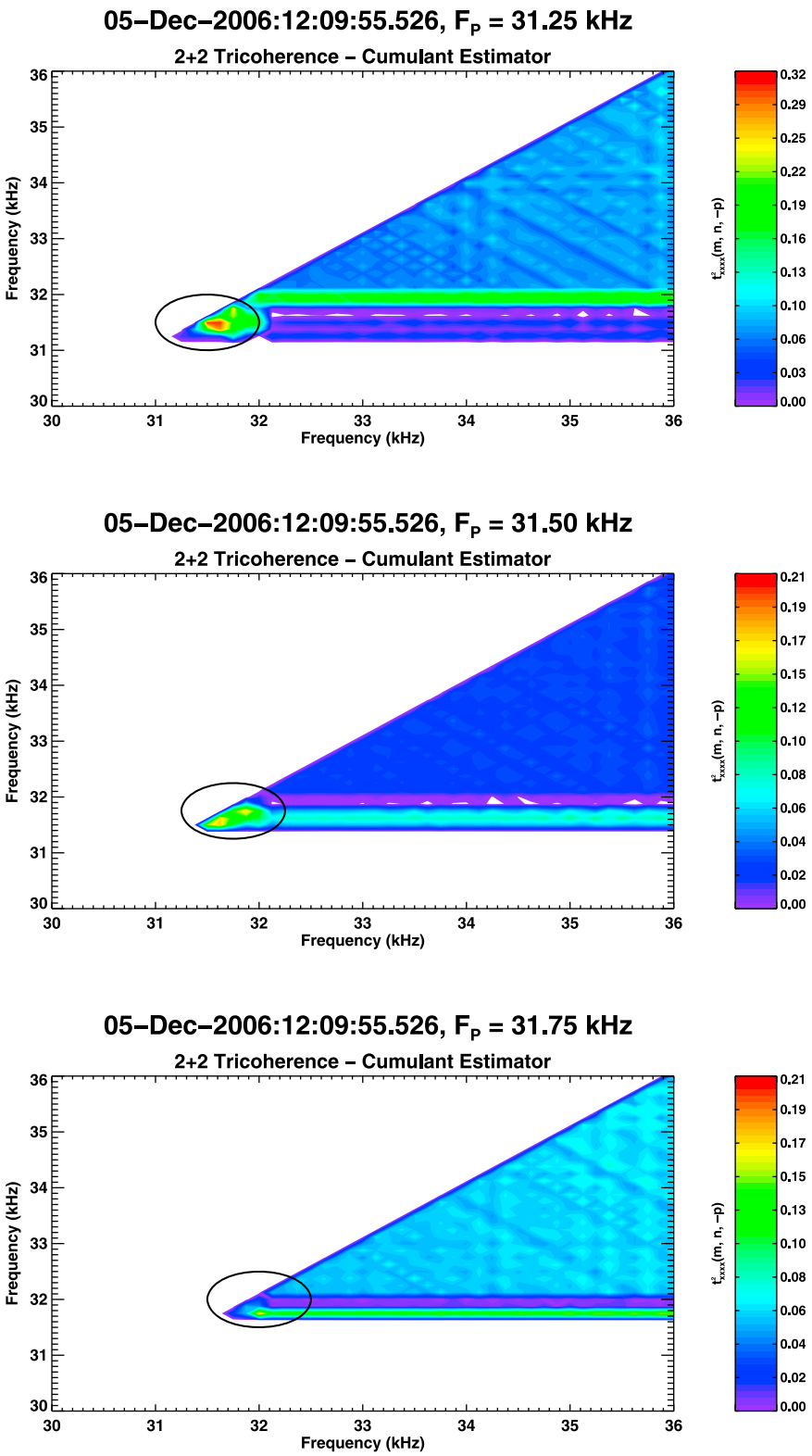

Figure 23. The cross-sections of the tricoherence spectrum of the TDS event of Figure 16, at (top) $F_p = f_D = 31.25$ kHz, (middle) $F_p = f_L = 31.50$ kHz, and (bottom) $F_p = f_U = 31.75$ kHz, where f_D, f_L and f_U are the frequencies of the down-shifted sideband, beam-excited Langmuir and up-shifted sideband modes, respectively.

[56] Thus, the significant tricoherences corresponding to $2\phi_L = \phi_D + \phi_U$ in the tricoherence spectra at Stokes, anti-Stokes and beam-excited Langmuir wave frequencies provide evidence for the modulational instability type of four-wave interactions in all the four events presented in this study.

4. Conclusions

[57] We have presented the observational evidence for the strong turbulence processes, namely, the supersonic modulational instability (MI), which is also known as the oscillating two stream instability (OTSI) and collapsing Langmuir solitons in the source regions of solar type III radio bursts. The high time resolution observations from the STEREO WAVES experiment show that the Langmuir waves excited by the electron beams occur as localized wave packets with durations less than ~10 ms and peak intensities exceeding the strong turbulence thresholds. These localized Langmuir wave packets satisfy the criterion of solitons collapsed to spatial scales of a few hundred Debye lengths. The spectra of these wave packets consist of intense peaks corresponding to beam-resonant Langmuir waves, two or more sidebands corresponding to Stokes and anti-Stokes modes, and low frequency enhancements below a few hundred Hz corresponding to ion sound waves. The frequencies and wave numbers of these spectral components satisfy the resonance conditions of the modulational instability. The tricoherence values are computed using the trispectral analysis techniques, which show that the spectral components of the wave packets are coupled to each other with a high degree of coherency, as expected of the MI. The observed high intensities, short scale lengths, sideband spectral structures and low frequency enhancements of the wave packets, and high levels of tricoherence amongst their spectral components strongly suggest that the wave packets are collapsing Langmuir solitons, and they are in the supersonic modulational instability regime. The implications of the observations presented in this study are that (1) the strong Langmuir turbulence processes occur in the source regions of solar type III radio bursts, (2) the supersonic modulational instability (MI) and spatial collapse probably play important roles in beam stabilization as well as conversion of Langmuir waves into escaping radiation at the fundamental and second harmonic of the electron plasma frequency, and (3) the Langmuir collapse in the case of type III bursts probably follows the supersonic modulational instability as suggested by *Zakharov* [1972].

[58] **Acknowledgments.** The research of T. G. is supported by the NASA Grants NNX08AO02G, NNX09AB19G and NNX12AH47G. The SWAVES instruments include contributions from the Observatoire of Paris, University of Minnesota, University of California, Berkeley, and NASA/GSFC. We thank the referees for constructive comments and helpful suggestions.

[59] Philippa Browning thanks the reviewers for their assistance in evaluating this paper.

References

Alvarez, H., R. P. Lin, and S. J. Bame (1975), Fast solar electrons, interplanetary plasma and km-wave type-III radio bursts observed from the IMP-6 spacecraft, *Sol. Phys.*, *44*, 485.

Bale, S. D., D. Burgess, P. J. Kellogg, K. Goetz, R. L. Howard, and S. J. Monson (1996), Phase coupling in Langmuir wave packets: Possible evidence of three-wave interactions in the upstream solar wind, *Geophys. Res. Lett.*, *23*, 109.

Balikhin, M., V. V. Krasnoselskikh, and L. J. C. Woolliscroft (1989), Reflection of electrons from the front of a strong quasi perpendicular shock and the generation of plasma waves, *Adv. Space Res.*, *9*, 203.

Balikhin, M. A., I. Bates, and S. Walker (2001), Identification of linear and nonlinear processes in space plasma turbulence data, *Adv. Space Res.*, *28*, 787.

Bardwell, S., and M. V. Goldman (1976), Three-dimensional Langmuir wave instabilities in type III solar radio bursts, *Astrophys. J.*, *209*, 912.

Benz, A. O. (2002), *Plasma Astrophysics: Kinetic Processes in Solar and Stellar Coronae*, Kluwer Acad., Dordrecht, Netherlands.

Bohm, D., and E. P. Gross (1949), Theory of plasma oscillations: A. Origin of medium-like behavior, *Phys. Rev.*, *75*, 1851.

Bougeret, J.-L., et al. (2008), S/WAVES: The radio and plasma wave investigation on the STEREO Mission, *Space Sci. Rev.*, *136*, 487.

Chandran, V., S. Elgar, and B. Vanhoff (1994), Statistics of tricoherence, *IEEE Trans. Signal Process.*, *42*, 12.

Cheung, P. Y., and A. Y. Wong (1985a), Periodic collapse and long-term evolution of strong Langmuir turbulence, *Phys. Rev. Lett.*, *55*, 1880.

Cheung, P. Y., and A. Y. Wong, (1985b), Nonlinear evolution of electron-beam plasma interaction, *Phys. Fluids*, *28*, 1538.

Dalle Molle, J. W., and M. J. Hinich (1989), The trispectrum, paper presented at Workshop on Higher-Order Spectral Analysis, IEEE, Vail, Colorado, 28–30 June.

Degtyarev, L. M., R. Z. Sagdeev, G. I. Solov'ev, V. D. Shapiro, and V. I. Shevchenko (1980), One-dimensional Langmuir turbulence, *Sov. J. Plasma Phys.*, *6*, 263.

Doolen, G. D., D. F. DuBois, and H. A. Rose (1985), Nucleation of cavitons in strong Langmuir turbulence, *Phys. Rev. Lett.*, *54*, 804.

DuBois, D. F., A. Hanssen, H. A. Rose, and D. Russell (1993), Space and time distribution of HF excited Langmuir turbulence in the ionosphere: Comparison of theory and experiment, *J. Geophys. Res.*, *98*, 17,543.

Ergun, R. E., et al. (1998) Wind spacecraft observations of solar impulsive electron events associated with solar type III radio bursts, *Astrophys. J.*, *503*, 435.

Ergun, R. E., et al. (2008), Eigenmode structure in solar-wind Langmuir waves, *Phys. Rev. Lett.*, *101*, 051101, doi:10.1103/PhysRevLett.101.051101.

Escande, D. F., and G. V. de Genouillac (1978), Electron burst relaxation in a fluctuating plasma, *Astron. Astrophys.*, *68*, 405.

Fainberg, J., and R. G. Stone (1971), Type III solar radio burst storms observed at low frequencies, *Sol. Phys.*, *17*, 392.

Fokker, A. D. (1984), Irregular paths of exciting electrons and the intensity-time profiles of type III bursts, *Sol. Phys.*, *93*, 379.

Galeev, V. V., and V. V. Krasnoselskikh (1976), Strong Langmuir turbulence in the Earth's magnetosphere as a source of kilometer radio emission, *Sov. Phys. JETP, Engl. Transl.*, *24*, 515.

Galeev, V. V., and V. V. Krasnoselskikh (1978), Mechanisms for the generation of radio waves by means of auroral electrons, *Sov. J. Plasma Phys.*, *4*, 62.

Galvin, A. B., et al. (2008), The Plasma and Suprathermal Ion Composition (PLASTIC) Investigation on the STEREO Observatories, *Space Sci. Rev.*, *136*, 437.

Ginzburg, V. L., and V. V. Zheleznyakov (1958), On the possible mechanisms of sporadic solar radio emission (radiation in an isotropic plasma), *Sov. Astron.*, *2*, 623.

Goldman, M. V. (1983), Progress and problems in the theory of type III solar radio emissions, *Sol. Phys.*, *89*, 403.

Goldman, M. V. (1984), Strong turbulence of plasma waves, *Rev. Mod. Phys.*, *89*, 403.

Goldstein, M. L., R. A. Smith, and K. Papadopoulos (1979), Nonlinear stability of solar type III radio bursts. Application to observations near 1 AU, *Astrophys. J.*, *237*, 683.

Gurnett, D. A., and R. R. Anderson (1976), Electron plasma oscillations associated with type III radio bursts, *Science*, *194*, 1159.

Gurnett, D. A., and R. R. Anderson (1977), Plasma wave electric fields in the solar wind: Initial results from Helios 1, *J. Geophys. Res.*, *82*, 632.

Gurnett, D. A., J. E. Maggs, D. L. Gallagher, W. S. Kurth, D. J. Williams, and F. L. Scarf (1981), Parametric interaction and spatial collapse of beam driven Langmuir wave in the solar wind, *J. Geophys. Res.*, *86*, 8833.

Gurnett, D. A., G. B. Hospodarsky, W. S. Kurth, D. J. Williams, and S. J. Bolton (1993), Fine structure of Langmuir waves produced by a solar electron event, *J. Geophys. Res.*, *98*, 5631.

Hasselman, K., W. Munk, and G. MacDonald (1963), Bispectra of ocean waves, in *Time Series Analysis*, edited by M. Rosenblatt, p. 125, John Wiley, New York.

Henri, P., C. Briand, A. Mangeney, S. D. Bale, F. Califano, K. Goetz, and M. Kaiser (2009), Evidence for wave coupling in type III emissions, *J. Geophys. Res.*, *114*, A03103, doi:10.1029/2008JA013738.

Heyvaerts, J., and G. V. de Genouillac (1974), Effects of turbulence anisotropy on propagation and electromagnetic radiation of particle streams in the solar corona, *Astron. Astrophys.*, *30*, 211.

Hospodarsky, G. B., and D. A. Gurnett (1995), Beat-type Langmuir wave emissions associated with a type III solar radio burst: Evidence of parametric decay, *Geophys. Res. Lett.*, *22*, 1161.

Kaplan, S. A., and V. N. Tsytovich (1968), Radio emission from beams of fast particles under cosmic conditions, *Sov. Astron.*, *11*, 956.

Kellogg, P. J., K. Goetz, R. L. Howard, and S. Monson (1992), Evidence for Langmuir wave collapse in the interplanetary plasma, *Geophys. Res. Lett.*, *19*, 1303.

Kellogg, P. J., K. Goetz, S. J. Monson, S. D. Bale (1999), A search for Langmuir solitons in the Earth's foreshock, *J. Geophys. Res.*, *104*, 6751.

Kellogg, P. J., K. Goetz, S. J. Monson, S. D. Bale, M. J. Reiner, and M. Maksimovic (2009), Plasma wave measurements with STEREO S/WAVES: Calibration, potential model, and preliminary results, *J. Geophys. Res.*, *114*, A02107, doi:10.1029/2008JA013566.

Kim, Y. C., and E. J. Powers (1979), Digital bispectral analysis and its applications to nonlinear wave interactions, *IEEE Trans. Plasma Sci.*, *7*, 120.

Krasnoselskikh, V. V., and V. I. Sotnikov (1977), Plasma-wave collapse in a magnetic field, *Sov. J. Plasma Phys.*, *4*, 491.

Kravtchenko-Berejnoi, V., F. Lefeuvre,V. Krasnoselskikh, and D. Lagoutte (1995a), On the use of tricoherent analysis to detect non-linear wave-wave interactions, *Signal Process.*, *42*, 291.

Kravtchenko-Berejnoi, V., V. V. Krasnoselskikh, D. Mourenas, and F. Lefeuvre (1995b), Higher-order spectra and analysis of a non-linear dynamic model, in *Proceedings of the Cluster Workshops, Data Analysis Tools and Physical Measurements and Mission-Oriented Theory*, edited by K.-H. Glassmeier, U. Motschmann, and R. Schmidt, *Eur. Space Agency Spec. Publ.*, *ESA SP-371*, 61.

Lefeuvre, F., V. Kravtchenko-Berejnoi, and D. Lagoutte (1995), Higher-order spectra and analysis of a non-linear dynamic model, in *Proceedings of the Cluster Workshops, Data Analysis Tools and Physical Measurements and Mission-Oriented Theory*, edited by K.-H. Glassmeier, U. Motschmann, and R. Schmidt, *Eur. Space Agency Spec. Publ.*, *ESA SP-371*, 51.

Lin, R. P. (1970), The emission and propagation of 40 keV solar flare electrons, *Sol. Phys.*, *12*, 266.

Lin, R. P., L. G. Evan, and J. Fainberg (1973), Simultaneous observations of fast solar electrons and type III radio burst emission near 1 AU, *Astrophys. Lett.*, *14*, 191.

Lin, R. P., D. W. Potter, D. A. Gurnett, and F. L. Scarf (1981), Energetic electrons and plasma waves associated with a solar type III radio burst, *Astrophys. J.*, *251*, 364.

Lin, R. P., W. K. Levedahl, W. Lotko, D. A. Gurnett, and F. L. Scarf (1986), Evidence for nonlinear wave-wave interactions in solar type III radio bursts, *Astrophys. J.*, *308*, 954.

Magelssen, G., and D. F. Smith (1977), Non relativistic electron stream propagation in the solar atmosphere and type III radio bursts, *Sol. Phys.*, *55*, 211.

McFarland, M. D., and A. Y. Wong (1997), Spectral content of strong Langmuir turbulence in the beam plasma interaction, *Phys. Plasmas*, *4*, 945.

McFarland, M. D., and A. Y. Wong (2001), Spatial, spectral, and statistical properties of the high-frequency electrostatic fluctuations in a beam-driven turbulent plasma, *Phys. Plasmas*, *8*, 110.

Michel, J. A., P. J. Paris, M. Schneider, and M. Q. Tran (1982), Nonlinear effects in a beam plasma system: Second harmonic emission and density depression formation, *Phys. Scr. T*, *1982*, 571.

Montgomery, D. A., R. P. Johnson, J. A. Cobble, J. C. Fernandez, H. A. Rose, and K. E. Estabrook (1999), Characterization of plasma and laser conditions for single hot spot experiments, *Laser Part. Beams*, *17*, 349.

Nicholson, D. R., M. V. Goldman, P. Hoyang, and J. C. Weatherall (1978), Nonlinear Langmuir waves during type III solar radio bursts, *Astrophys. J.*, *223*, 605.

Nikias, C. L., and M. R. Raghuveer (1987), Bispectrum estimation: A digital signal processing framework, *Proc. IEEE*, *75*, 869.

Ogilvie, K. W., et al. (1995), A comprehensive plasma instrument for the wind spacecraft, *Space Sci. Rev.*, *71*, 55.

Papadopoulos, K., M. L. Goldstein, and R. A. Smith (1974), Stabilization of electron streams in type III solar radio bursts, *Astrophys. J.*, *190*, 175.

Papagiannis, M. D. (1971), Studies of the outer corona through space radio astronomy, in *Physics of the Solar Corona: Proceedings of the NATO Advanced Study Institute, held at Cavouri-Vouliagmeni, Athens, September 6–17, 1970*, vol. 27, edited by C. J. Macris, p. 317, D. Reidel, Dordrecht, Netherlands.

Pelletier, G., H. Sol, and E. Asseo (1988), Generation of a high-energy electron tail by strong Langmuir turbulence in a plasma, *Phys. Res. Lett.*, *38*, 2552.

Robinson, P. A. (1997), Nonlinear wave collapse and strong turbulence, *Rev. Mod. Phys.*, *69*, 507.

Russell, D. A., D. F. DuBois, and H. A. Rose (1988), Nucleation in two-dimensional Langmuir turbulence, *Phys. Rev. Lett.*, *60*, 581.

Smith, R. A., M. L. Goldstein, and K. Papadopoulos (1979), Nonlinear stability of solar type III radio bursts: I. Theory, *Astrophys. J.*, *234*, 348.

Soucek, J., T. Dudok de Wit, V. Krasnoselskikh, and A. Volokitin (2003), Statistical analysis of nonlinear wave interactions in simulated Langmuir turbulence data, *Ann. Geophys.*, *21*, 681.

Sturrock, P. A. (1964), Type III solar radio bursts, in *Proceedings of a Symposium Held at the Goddard Space Flight Center, Greenbelt, Maryland, October 28–30, 1963*, edited by W. N. Hess, *NASA Spec. Publ.*, *50*, 357.

Takakura, T., and H. Shibahashi (1976), Dynamics of a cloud of fast electrons traveling through the plasma, *Sol. Phys.*, *46*, 323.

Thejappa, G., and R. J. MacDowall (1998), Evidence for strong and weak turbulence processes in the source region of a local type III radio burst, *Astrophys. J.*, *498*, 465.

Thejappa, G., and R. J. MacDowall (2004), High frequency ion sound waves associated with Langmuir waves in type III radio burst source regions, *Nonlinear Processes Geophys.*, *11*, 411.

Thejappa, G., D. Lengyel-Frey, R. G. Stone, and M. L. Goldstein (1993a), Evaluation of emission mechanisms at ω_{pe} using Ulysses observations of type III bursts, *Astrophys. J.*, *416*, 831.

Thejappa, G., D. Lengyel-Frey, R. G. Stone, and M. L. Goldstein (1993b), Evaluation of solar type III burst theories using Ulysses URAP observations, in *Physics of Space Plasmas*, edited by T. Chang and J. R. Jasperse, p. 517, URAP, Berkeley, Calif.

Thejappa, G., D. Wentzel, and R. G. Stone (1995), Low-frequency waves associated with Langmuir waves in solar wind, *J. Geophys. Res.*, *100*, 3417.

Thejappa, G., R. G. Stone, and M. L. Goldstein (1996), Detection of Langmuir solitons: Implications for type III burst emission mechanisms at $2\omega_{pe}$, *Astrophys. Space Sci.*, *243*, 195.

Thejappa, G., M. L. Goldstein, R. J. MacDowall, K. Papadopoulos, and R. G. Stone (1999), Evidence for Langmuir envelope solitons in solar type III radio burst source regions, *J. Geophys. Res.*, *104*, 28,279.

Thejappa, G., R. J. MacDowall, E. E. Scime, and J. E. Littleton (2003), Evidence for electrostatic decay in the solar wind at 5.2 AU, *J. Geophys. Res.*, *108*(A3), 1139, doi:10.1029/2002JA009290.

Thejappa, G., R. J. MacDowall, M. Bergamo, and K. Papadopoulos (2012a), Evidence for the oscillating two stream instability and spatial collapse of Langmuir waves in a solar type III radio burst, *Astrophys. J.*, *747*, L1.

Thejappa, G., R. J. MacDowall, and M. Bergamo (2012b), Phase coupling in Langmuir wave packets: Evidence of four wave interactions in solar type III radio bursts, *Geophys. Res. Lett.*, *39*, L05103, doi:10.1029/2012GL051017.

Thornhill, S. G., and D. ter Haar (1978), Langmuir turbulence and modulational instability, *Phys. Rep.*, *43*, 43.

Vyacheslavov, L. N., V. S. Burmanov, I. V. Kandaurov, E. P. Kruglyakov, O. I. Meshkov, and A. L. Sanin (2002), Dissipation of strong Langmuir turbulence in non isothermal non-Maxwellian plasma, *JETP Lett.*, *75*, 41.

Walker, S. N., M. A. Balikhin, I. Bates, and R. Huff (2002), An investigation into instrumental nonlinear effects, *Adv. Space Res.*, *30*, 2815.

Walker, S. N., J. S. Pickett, D. A. Gurnett, and H. Alleyne (2003), High order spectral analysis of electron plasma oscillations in the electron foreshock, *Adv. Space Res.*, *32*, 309.

Whelan, D. A., and R. L. Stenzel (1981), Electromagnetic-wave excitation in a large laboratory beam-plasma system, *Phys. Rev. Lett.*, *47*, 95.

Wong, A. Y., and P. Y. Cheung (1984), Three-dimensional self-collapse of Langmuir waves, *Phys. Rev. Lett.*, *52*, 14.

Zaitsev, V. V., N. A. Mityakov, and V. O. Rapoport (1972), A dynamic theory of type III solar radio bursts, *Sol. Phys.*, *24*, 444.

Zaitsev, V. V., M. V. Kunilov, N. A. Mityakov, and V. O. Rapoport (1974), Generation of type III radio bursts by electron fluxes having a large injection time, *Sov. Astron., Engl. Transl.*, *18*, 147.

Zakharov, V. E. (1972), Collapse of Langmuir waves, *Sov. Phys. JETP, Engl. Transl.*, *35*, 908.

Zakharov, V. E., S. L. Musher, and A. M. Rubenchik (1985), Hamiltonian approach to the description of non-linear plasma phenomena, *Phys. Rep.*, *129*, 285.

Zheleznyakov, V. V., and V. V. Zaitsev (1970), Contribution to the theory of type III solar radio bursts. I., *Sov. Astron., Engl. Transl.*, *14*, 47.